Concepts, models and methods in computational heterogeneous catalysis illustrated through CO_2 conversion

Ángel Morales-García,[1] Francesc Viñes,[1] José R. B. Gomes,[2] and Francesc Illas[1,*]

[1]*Departament de Ciència de Materials i Química Física & Institut de Química Teòrica i Computacional (IQTCUB), Universitat de Barcelona, C/Martí i Franquès 1-11, 08028 Barcelona, Spain.*

[2]*CICECO – Aveiro Institute of Materials, Department of Chemistry, University of Aveiro, Campus Universitário de Santiago, 3810-193 Aveiro, Portugal.*

* Corresponding author: francesc.illas@ub.edu

Abstract

Theoretical investigations and computational studies have notoriously contributed to the development of our understanding of heterogeneous catalysis during the last decades, when powerful computers have become generally available and efficient codes have been written that can make use of the new highly parallel architectures. The outcome of these studies has shown not only a predictive character of theory but also provide inputs to experimentalists to rationalize their experimental observations and even to design new and improved catalysts. In this review, we critically describe the advances in computational heterogeneous catalysis from different viewpoints. We firstly focus on modelling because it constitutes the first key step in heterogenous catalysis where the systems involved are tremendously complex. A realistic description of the active sites needs to be accurately achieved to produce trustable results. Secondly, we review the techniques used to explore the potential energy landscape and how the information thus obtained can be used to bridge the gap between atomistic insight and macroscale experimental observations. This leads to the description of methods that can describe the kinetic aspects of catalysis, which essentially encompass microkinetic modelling and kinetic Monte Carlo simulations. The puissance of computer simulations in heterogeneous catalysis is further illustrated by choosing CO_2 conversion catalysed by different materials for most of which a comparison between computational information and experimental data is available. Finally, remaining challenges and a near future outlook of computational heterogeneous catalysis are provided.

Keywords: Computational catalysis, DFT, microkinetic, kinetic Monte Carlo, CO_2 conversion

1. Introduction

The need for a sustainable society requires that chemical commodities are obtained in an environmentally, friendly and energy efficient way, and this can only be achieved by means of efficient catalytic processes with high activity and selectivity at mild conditions. Leaving enzymes apart, catalysts can be roughly classified into homogeneous and heterogeneous, depending on whether the process takes place in one or more phases. Homogeneous and heterogeneous catalysts have pros and cons, the former usually exhibiting higher catalytic activities but, in general, being less stable and more difficult to reutilize, apart from separation issues that are far from being trivial. For large-scale production of useful chemicals, catalysts must be also stable and durable, resistant to sintering and poisoning species, and easily recovered and regenerated.[1] These are advantageous properties of heterogeneous solid catalysts and the reasons why they are broadly used for the continuous operation in chemical industries.

Most of the current heterogeneous catalysts were found by trial-and-error approaches, which required time consuming experiments for the preparation and testing of potential candidates for a given reaction. With a few exceptions, as the case of pure metals or binary oxides, catalysts are generally obtained by mixing several different reagents, usually under harsh temperature and pressure conditions, resulting in very complex structures.[2,3] There are several different kinds of solid catalysts,[1,2] either based or supported on a given substrate, involving pure metals or metal alloys, binary or mixed oxides, multicomponent oxides as the broadly used zeolites, carbides, nitrides, sulphides, carbons, metal salts, hybrid materials such as metal organic frameworks, or periodic mesoporous organosilicas, and the recently discovered family of MXenes. In most catalysts, the nature of the active sites is not well understood, specially under *operando* conditions, and unanimity is rare about reaction mechanisms and/or formed intermediate species. Thus, with so many unknowns, the optimization of existing catalysts is not trivial, and finding of new ones involves time-consuming and expensive experiments. Microscopic understanding is surely a way to the rational design of catalysts and efforts in this direction have been addressed from experimental and theoretical sides.

The elucidation of the reaction mechanisms occurring at the catalyst surface requires significant knowledge about the surface structure and the surface chemistry. For a long time, detailed experimental spectroscopic, diffraction, and microscopic studies aimed at the identification of reaction sites and analysis of the formed reaction intermediates and products. This has been accomplished under ultra-high vacuum conditions on well-defined single crystal surfaces that have been used as catalyst models.[4] Recent advances have been enabling the study of more complex, hence realistic, systems, and to predict catalysis under *operando* conditions. The experimental data were employed to benchmark results from *ab initio* theoretical methods and to aid the development of novel computational frameworks, in special methods based on the density functional theory (DFT), which have been used to predict adsorbate-surface structures, to elucidate reaction mechanisms and to propose descriptors that can facilitate the screening of potential new and improved catalysts.[5]

The need for improved, more active, and selective catalysts is clear when realizing that human activities are the main responsible of the emissions of the greenhouse gases in the atmosphere over the last 150 years. Catalysts have been very useful to enhance production efficiency and reduce energy use and they may be key in transforming greenhouse gases into useful chemicals thus being able to contribute to a circular economy. Among the greenhouse gases, carbon dioxide (CO_2) is considered the main actor in the well-known global warming, even though its lower global warming potential (GWP = 1) when compared with methane (CH_4, GWP = ~30), nitrous oxide (N_2O, GWP = ~ 280), or fluorocarbons derivatives (GWP > 1000);[6] this clearly indicates the tremendous amounts of CO_2 that have been sent to the atmosphere because of burning fossil fuels (*e.g.*, transportation, electricity production, etc.), or production of goods (*e.g.*, cement industries).[7] At present, the current global atmospheric CO_2 concentration is *ca.* 415 ppm as measured at the National Oceanic and Atmospheric Administration (NOAA´s Mauna Loa Observatory on Hawai;[8] furthermore, 36.44 billion tonnes of CO_2 come directly from burning fossil fuels and cement production.[9] The latter indicator is estimated to decrease ~8% in 2020 as consequence of the Covid-19 pandemics. Despite this, to keep the rise in global temperatures, emissions of carbon dioxide would have to be cut significantly from 2020 onwards. In fact, in December 2015, approximately two-hundred Governments that participated in the 6th Annual Sustainable Innovation Forum, held in Paris,[10] adopted the

Paris agreement —the first-ever universal, legally binding global climate change agreement— with the aim of undertaking rapid reductions of greenhouse gas emissions for limiting global warming to well below 2 ºC above pre-industrial levels in the year 2100. In accordance with the most recent scientific advances, the plan arising from the agreement intends a balance between emissions and removals by 2050, *i.e.*, an economy with net-zero greenhouse gas emissions. Therefore, it is of utmost importance to optimize existing or to develop new chemical processes that are environmentally greener and more sustainable, relying essentially on renewable energy from clean and constantly replenished natural sources based on heterogeneous catalysis. In particular, it is expected that the contribution from computational modelling will contribute to speed-up the discovery of the needed new catalysts, given their in-depth analysis power.[11] Herewith, we seek to provide an account of structural models and computational methods currently used in computational heterogenous catalysis and to examine their full potential to advance our knowledge about the reactivity, selectivity and reaction mechanisms of catalysts proposed for CO_2 conversion into valuable products.

2. From ideal to realistic structural models

The atomistic modelling of a catalyst together with the methodology applied to predict its properties are two critical aspects defining the quality, and eventually the usefulness, of any given computational simulation. Ideally, one would seek for a representative model of the system under study, and treat it with a methodology that provides accurate and reliable results. However, whenever one of these two aspects is not fully met, the risk is getting partial, or even irrelevant information. For instance, a model distant from the reality could be treated accurately, but the results, even if certain for the chosen model, cannot —and should not— be related to the system of interest. On the other hand, a correct model, but treated with an insufficiently accurate methodology may deliver untrustworthy, and so less meaningful results. The worst case is, obviously, a poor model treated with an unsuited methodology, which simply offers nonsense results.

The above apparently naïve description is core on a planned simulation. Realistic models treated with highly accurate methodologies are still not a solution because there are limits both on the number of atoms to be explicitly included in the model and on the

theoretical methodology, both being strongly related to the available computational resources. For instance, simulations of systems containing thousands of atoms by means of classical molecular dynamics (MD) using a non-reactive force field is standard nowadays, affordable even using desktop computers.[12] However, an all-electron DFT study of systems with thousands of atoms is barely achievable nowadays.[13] In fact, such calculations require highly parallelized codes such as the Fritz-Haber institute *ab initio* simulation package (FHI-AIMS) [14] and, simultaneously, high parallel supercomputers with thousands of connected nodes and processors, which are not always at disposal.

Besides, when the interest implies dynamical aspects, the time of the simulation is and additional factor to take into account. For instance, even the more accessible MD simulations are challenged when one has to deal with millions of atomic coordinates in a given model, or, on the other side, a MD run of a suitable model of a thousand atoms is challenged when pretending to run μs simulations with a fs timestep. This is simplified in size and time scales in Figure 1, revealing that to increase time and/or size of the studied system requires going to a less accurate methodology. Furthermore, notice that the employed model and methodology go by hand-to-hand, as the model size already delimits the type of methodology that can be currently applied. In the next subsections we address the most common and utilized models, from a time and evolution perspective.

2.1. Catalyst models: Cluster vs. periodic

When simulating a heterogeneous catalyst, a central, key point is the modelling of the catalyst material, particularly, of its exposed surfaces and surface defects and species, as they will be the part in contact with the reaction reagents, intermediates, and products. Two main approaches are commonly used when modelling a catalyst material; these are the cluster and the periodic models. Historically, cluster models were firstly developed and employed, due to their simplicity, which allow applying all sorts of wave-function based methods, up to the computationally highly expensive coupled-cluster single double and perturbative triples level of theory, *i.e.* CCSD(T), often recognized as a golden standard of accuracy by the quantum chemistry community.[15] To investigate the chemistry of cluster models, the electronic structure modeller can make use of available molecular codes such as Gaussian,[16] Turbomole,[17] NWChem,[18] Orca,[19] Gamess-US,[20] among many others.

The intricacy of cluster models lies then on the suitability to represent the system of interest and the property to be explored. Original research approached the materials surface by a single atom, as done, for instance, in analysing the carbon dioxide (CO_2) interaction with alkali atoms, transition metal cations and anions,[21-24] and possible formation of carbon monoxide (CO), or even the effect of binary model catalytic centres, like on a metal oxide unit.[25] When a single atom is used to describe the catalytic active centre, see Figure 2a, one must realize that the electronic structure of a catalytic active atom in a catalyst is different from that of the isolated atom in gas phase. Apart from differences in the electronic ground state, that for an isolated atom will for sure involve open-shells, its catalytic activity is modulated by the surrounding atoms, which can indirectly affect its electronic structure, similarly to the ligand effect, or do indeed participate in the interaction with the reaction species. In that case, the surrounding atoms should be included in the models as they are part of the catalytic active site. In general, it is more practical to use cluster models of a few atoms in the actual description of the catalytic active centres, see Figure 2a. Indeed, gas phase or supported, small clusters can be regarded as explicit models, as they have been extensively studied both from the experimental and theoretical sides.[26-28] In addition, these small clusters can be experimentally deposited or grown on a support and then used as catalyst models. Here, soft-landing techniques have been used to control the size of the deposited clusters.[29,30]

However, the utilization of small clusters is not exempt of dangers. The lack of bonds between cluster atoms and those that exist in the material, which are neglected in the model, leads to a significant number of low-coordinate atoms with concomitant high-in-energy electronic structures. Indeed, this instability is the driving force towards large structural deformations when the atomic structure of such a cluster model is fully optimized, particularly fostered by the large number of low lying structural isomers which exist in a narrow energy range, which are normally achievable through low energy barriers, pointing out their fluxionality.[28,31] To avoid these problems the structure of the cluster models is normally kept as in the catalyst structure, often at the bulk experimental or theoretical optimized positions.[32] A different situation appears when one pretends to model larger systems, such as large nanoparticles (NPs), allowing for the versatile description of regular surface sites and even defective sites, such as corner, edge, step, or kink sites, see Figure 2a.

Here, depending on the cluster size and on the goal of the simulation, one can make use of the optimized structure even if neglecting the effect of the underlying substrate.

In the case of extended metallic systems, the use of small clusters forces a localized electronic structure, which is unnatural for an otherwise delocalized electronic structure system. Such a quantum confinement of the electron density leads normally to an enhanced chemical activity, which can be minimized by simply using larger models either cut from the bulk or in the form of NPs, as explained later, although efficient embedding schemes have been proposed that minimized the edge effects.[33] In the case of ionic systems, one lacks the effect of the Madelung electrostatic potential as generated for the more distant ions. This missing piece can be solved by including point charges surrounding the studied cluster,[34-36] while counteracting possible polarizations at the interface between the explicit cluster and the point charges.[37,38] When it comes to covalent systems, zeolites and silicas being paradigmatic examples, the broken bonds when creating the cluster leave high-in-energy dangling bonds, which may lead to unrealistic electronic structures, or, if optimized, to large structural rearrangements. To avoid so, normally such dangling bonds effect is cancelled by terminating such atom with covalent bonds with capping hydrogen atoms.[38,39]

Thus, the proper description of the catalytic active centre surrounding atoms is pivotal in a good description, either to allow an electronic delocalization, to account for the Madelung electrostatic potential effect, or to properly describe covalent bonds. This particular point is what made simulations under periodic boundary conditions (PBC) so popular in the last couple of decades. The underlying idea is to use the theoretical framework as used in the description of crystalline bulk unit cells to model surfaces and other surface centres. Because of this, as in a bulk environment, see Figure 2a, one requires defining the unit cell lattice vectors and shape, and one ends carrying out the numerical integrations in the reciprocal unit cell, as a consequence of the Bloch theorem treating periodicity in crystal structures.[40] This forces the exploration of the **k**-point space in which the electronic states are evaluated, and frequently dealt with a regular mesh of **k**-points, dense enough so as to provide converged energy results. Also, for consistency, the bulk material is normally optimized, and from that, either cluster models are cut, or periodic models are built.

The use of PBC has the tremendous advantage of including the effect of the *infinite* material on the catalytic active centre, and hence, large clusters, point charges, or embedding H atoms are not required to get reliable results. Indeed, the computational costs can be greatly reduced when using the primitive unit cell; for instance, regular rock-salt bulk crystal structures can be described having only four atoms in the unit cell. However, the use of PBC has its drawbacks; for instance, the necessity of having periodic wavefunctions popularized the use of plane-waves as a basis set, such as in the Vienna *ab initio* simulation package (VASP) code,[41] but its use is detrimental when carrying out wavefunction based calculations, *e.g.*, Hartree-Fock calculations, and also when making use of hybrid functionals involving a fraction of the Fock exchange. Other periodic codes, such as CRYSTAL,[42] or the FHI-AIMS,[14] circumvent this issue using atomic orbitals as wave functions either analytic or numerical, respectively.

One must also point out that, the simulation of low-coverages situations or particular surface defects may require large supercells to avoid the lateral interaction of replicated surface species or defects, which can well lead to highly demanding simulations of hundreds of atoms, which, in turn, can be unfeasible depending on the employed code, method, and the available computational resources one would have. The peculiarities of such PBC models are treated in more detail in the explicit models described in the next section. Before closing this section, we want to highlight that, to a large extent, the cluster model approach has been mainly used for interpretative purposes. In fact, it is still used to understand activation and reaction of CO_2 to other carbonaceous compounds on complicated adsorbents where other models cannot be easily used.[43,44]. In addition, we believe that the cluster model approach it is likely to play a significant role in the description of photocatalysis, where one needs to describe the reaction in a particular excited state potential energy surface, most likely using appropriate explicitly correlated wave functions.[45,46]

2.2. Exemplary models

As introduced in the previous section, clusters were the original models used in theoretical heterogeneous catalysis. These dominated the study of adsorbate↔surface interactions, and seminal catalytic reaction descriptions mainly in the 15 years spanning the 1980-1995

period.[39,47] As above briefly introduced, the cluster edge effects may have a strong impact on the cluster electronic structure, and, eventually, affect its surface and catalytic properties, delivering strong oscillations with cluster size on inherent properties such as cohesive energies, or activity properties such as adsorption energies. The structural and electronic structure of these cluster models can significantly differ from those of the bulk material or of larger realistic NPs. Yet, small clusters may be indeed present in the real catalyst and, in this respect, the cluster structure optimization and the quests for finding global minima as a function of size are recurrent studies, approached using global optimization techniques such as basin-hopping or evolutionary algorithms, normally profiting from suited interatomic potentials to lower the computational burden. Given the vast literature on the field, we address the reader to excellent reviews.[26,48-50]

Conversely, it is worth pointing out that, to a large extent, edge effects on cluster models directly cut from bulk are the responsible for strong oscillations on inherent and surface properties. In part, this can be avoided by larger clusters, as in metallic NPs of 1-10 nm size, where delocalization of the electronic structure is allowed or in ionic systems where the Madelung electrostatic potential builds up. A good strategy to minimize the edge effects is by using NPs with shapes that minimize the surface energy. This is achieved by relying on the Wulff construction.[51] This requires utilizing the surface energies γ of (*hkl*) planes that can be routinely acquired using slab models. Since the total energy of a surface is given by the product of the surface energy γ by the surface area *A*, one ends up assuming an equilibrium structure so that $\int \gamma(hkl) \cdot \mathrm{d}A(hkl) = \text{minimum}$ for all the exposed surfaces; see an example of a metallic Wulff NP in Figure 2a. For a step-by-step description of Wulff theorem and its application to the generation of NPs, we refer to excellent reviews and books available in the literature,[52,53] where even more sophisticated approaches considering edge and corner energies contributions are described, also treating bulk elasticity and relevant conditions of temperature and surface composition.[54]

The Wulff construction allows one generating models with tailored shapes and exhibiting well-defined facets; computer codes are freely available for an automatic generation of NPs.[55] Here, the scalability concept becomes tremendously useful, as numerous studies in the past revealed that the strong oscillations, as observed in the small

cluster models, disappear when using larger, well-shaped NPs.[53,56] This allows having properties either converged with size, as the case of adsorption energies, or that linearly scale with the NP size, normally sized by $n^{-1/3}$, where n is the number of atoms of the NP, see Figure 2b. The fact that scalable or converged results are obtained validates the utilization of NP models, also called nanocrystallites, to represent larger NPs of similar morphology. Notice, however, that different scalability onsets are found for different properties and different materials, and so, a validation check is required depending on the system and property prior to the scalability utilization.

The computational cost of treating NPs in the scalable regime, normally containing ~100-200 atoms, becomes very high, particularly when carrying out all electron calculations, which forced the exploitation of NP symmetry constraints.[57,58] The development of highly parallelized codes and the access to supercomputers with thousands of cores allows geometry optimization of large NPs without needing to restrain their symmetry.[53,56] For instance, all-electron DFT calculations for the geometry optimization of NPs containing from hundreds up to thousands of atoms have been reported for oxide nanostructures such as TiO_2 and ZnO.[13,59-61] In these NPs, the shape, stoichiometry and polar surface endings are properly treated. Thus, the simulation of NPs of different types of materials within the scalable regime has become a standard, and popularized the study of their catalytic reactivity in all sorts of reactions.[58,62-64] More importantly, given their realistic size, these NPs constitute appropriate explicit models of experimental NPs, particularly when they are located in the 1-5 nm size region.

On the other side, the PBC models evolved towards the description of surfaces through the so-known slab model, see Figure 2a, which has dominated the heterogeneous catalysis field from 1995 onwards.[65-67] Within the slab model, a periodic unit cell is built containing a given number of materials layers. Depending on the basis set and computational code used, a vacuum region may need to be added perpendicular to the modelled surface plane. Concerning the slab model, different approaches are used concerning the atomic relaxation. Originally, asymmetric slabs were employed, where the layers in contact with the reactants are optimized, while the other ones are kept at bulk positions, this is, to correctly describe the bulk environment. Other approaches consider all atomic layers fixed, all relaxed, or a symmetric slab where both ending surfaces

terminations are relaxed, while some layers in the middle of the slab are kept at the bulk positions to provide an appropriate environment. Notice that such slab models require convergence tests of the properties of study, *e.g.*, adsorption energies or reaction energy barriers, with respect the number of layers contained in the slab, and the added vacuum space. In general, there is not a single recipe since the model must represent realistically the system of interest and capture appropriately the specific properties to be investigated.

The use of slab models, given their possibilities, accessibility, and moderate computational expenses, has become the *de facto* workhorse in the last two decades; particularly when modelling reactivity at high coverage regimes of the clean surfaces,[68-70] although lately the increased computational resources allowed studying situations at a low coverage,[71 - 73] and including also surface defects such as vacancies,[74 - 76] subsurface species,[77-79] surface atoms,[80-82] etc. Notice that slab models also permit to represent regular defects, such as surface steps, see Figure 2a, by using vicinal surfaces slab models,[83-85] allowing also chemical resolution studies on chiral surfaces.[86-88]

One particular appealing aspect to have in mind is that different slab models can be combined so as to provide a more holistic description of more complex systems such as supported large NPs, particularly weighting the results by the Wulff proportions of surfaces under *operando* reaction conditions.[89-91] Likewise, slab models can be complemented with nanocrystallite models, so as to accurately describe NPs extended facets and low-coordinated sites such as edges and corners. Indeed, such nanocrystallites can be modelled directly using a molecular code or under PBC placing them in a large cubic cell with added vacuum in all three directions, so that the same computational setup and basis set can be employed on both the surface and NP model, allowing for a better, direct comparison.[92-95]

Last but not least, slab supercell models allow one to model more complex structures permitting, for instance, to approach supported catalysts. Hitherto, studies for supported NPs on different oxide substrates have been reported, including Pd and Pt NPs on MgO(001),[96] and Pt NPs on ZrO_2(111),[97] and $SrTiO_3$(001).[98] However, to model large supported NPs of size *ca.* 2 nm and sufficiently isolated from each other requires very large supercells and, consequently, very large computational resources. More recently, the advances on heterogeneous catalysis have been focused on metal NPs on oxide supports.[99-

[101] This has motivated the study of small supported clusters containing roughly 10-50 atoms as shown in the recent literature. [102 - 104] These systems have practical interest as experimental efforts are being pursued towards the synthesis of single atoms catalysts (SACs) as well as few-atom catalysts (FACs).[105,106] Here, experiment and computational models nicely converge with a promising feedback between them.

3. Exploring the potential energy surface

Heterogeneous catalysis denotes processes in which the phase of the catalyst and reactants differs because the reaction involves gas (or liquid) phase molecules adsorbing on a solid surface. As in any chemical process, the overall reaction usually consists of a series of elementary steps, the key point here is that most of them occur on the catalyst surface. Unveiling the microscopic mechanism of a chemical reaction requires exploring in detail the corresponding potential energy surface (*PES*). In the case of heterogeneously catalyzed reactions, this implies understanding adsorption, diffusion of reactants through the surface of catalyst, bond breaking and bond forming to generate reaction intermediates and products, and their eventual desorption from the catalyst. Not surprisingly, these complex processes demand tasks to establish a deep knowledge at atomistic-level of the catalyst to identify the main intermediates and surface sites involved in the reaction in a space- and time-dependent multiscale approach.[107,108]

To this purpose, theoretical calculations based on quantum chemistry have been broadly used as a fundamental tool to understand the reaction mechanisms and to investigate active sites on the catalytic surface.[109,110] In particular, DFT based methods allow one investigating reaction mechanisms occurring on the active solid surfaces.[111] The evaluation of reaction mechanisms involves (1) the conjecture of suitable pathways; (2) the geometrical optimization of the initial guesses, identifying stationary points in the PESs, locating and characterizing the local minima and transition states along each postulated reaction pathway (at 0 K); and, finally, (3) the inclusion of temperature and pressure effects through statistical thermodynamics. For the surface species, this requires the calculation of partition functions that include only vibrational degrees of freedom when treated in the harmonic approximation. For the gas-phase species, thermodynamic properties are obtained including all the degrees of freedom and assuming an ideal gas behavior.[5] This three-step

strategy allows one to obtain the Gibbs free energy surfaces at the reaction conditions of interest. It is worth pointing out that, on going from total energy to Gibbs free energy, the main effect is on the relative position of all intermediates while the energy barriers for each elementary step become almost unaffected simply because the difference in entropy for the initial state and the TS is usually very small. In this sense, total energy and Gibbs free energy barriers for a given molecular mechanism almost coincide.

In recent years, joint experimental and theoretical studies have become routine and have proven crucial to any fundamental understanding of catalysis at the molecular level.[112,113] The following subsections introduce briefly the computational models based on quantum chemistry methods, DFT approaches in particular, and their usage in computational heterogeneous catalysis.

3.1. Computational models

Theoretical Chemistry focuses on the mathematical description of Chemistry and in finding appropriate methods and algorithms to approach the properties of interest. The implementation of these algorithms in a computer generates the field generally known as Computational Chemistry. Indeed, Computational Chemistry really took off with the advent of mainframe computers during the 1960s.[114] Noting that just few aspects of Chemistry can be computed exactly, but almost every aspect of it has been described in a qualitative or approximate quantitative computational scheme.[115] One must keep in mind that numbers obtained from theoretical calculations are not exact, but they can offer a useful insight into real chemistry.[116]

Different computational methods use different levels of theory to produce results with different levels of accuracy. There are two main types of models depending on the starting point of the theory and on the properties that are to be described. On the one hand, one has classical methods that use Newton mechanics, these are applicable to model the structure of large molecular systems but are not adequate to problems involving bond breaking and bond making. On the other hand, one has the Quantum Chemistry methods, which makes use of Quantum Mechanics[117] and are of general application even if in practice there are limitations. Over the last decades, Quantum Chemistry has become an essential tool in designing new catalysts to ensure at this stage their highly activation and

selectivity including high turnover rates, while maintaining thermochemical stability, thereby decreasing the industrial cost.[109] These goals can be theoretically achieved or predicted at least by the underlying core technology that is the computational solution of the electronic Schrödinger equation.[118]

3.2. DFT flavors

Pierre Hohenberg and Walter Kohn showed that, for the electronic ground state of a non-degenerate system, the Schrödinger equation formulated as an equation of *N*-electron wavefunction of 3*N* spatial plus N spin variables, could be reformulated as an equation of the electron density with only three spatial variables.[119] This leads to the take-off of DFT methods that attempt to calculate the electronic ground total energy and other properties from the ground state electron density only. This formulation results in an enormous computational simplification, and systems with more than thousands of electrons can be treated by using DFT. An important step forward applying DFT to real systems was taken in 1965 when Kohn and Sham recast the Schrödinger equation for the electronic ground state into a problem of non-interacting electrons moving in an effective potential.[120] There are many distinct implementations to Kohn-Sham (KS) theory based on the choice of the structural model used to describe the studied system —see above in Section 2—, on the choice of basis set, and by the approximation employed in the treatment of the so-called exchange-correlation effects.[121]

To approach the solution of the KS equations, a basis set needs to be selected and the choice depends somehow on the models used to represent the system of interest and the properties to be investigated. For instance, localized functions are the usual choice in the above-described cluster-type models, whereas plane waves are most often used in slab-type calculations to simulate extended solids and surfaces.[122] Nevertheless, plane waves can also be used for cluster model calculations using a sufficiently large supercell and localized basis sets can be used in periodic DFT calculations with the appropriate code. Often, especially when using plane wave basis sets, the core electrons are not treated explicitly, but instead are included as ‘frozen’ densities represented in the appropriate basis set or through a pseudopotential that mimics the effect of the atomic core on the valence electron density. Fortunately, the error generated by the choice of a particular structural model can

be controlled and minimized easily upon building more realistic models in terms of size, shape, and environment where it operates. Similarly, the error derived from basis set can be controlled by increasing its quality up to the point of convergence. However, one needs to find a balance between catalyst model and computational method so as to avoid an excessive computational cost while maintaining a reasonable accuracy. This leaves the choice of exchange correlation functional as the main approximation in the DFT calculations.

3.3. Jacob's elevator to computational heterogeneous catalysis

The objective of DFT methods in the KS implementation is to develop accurate exchange correlation density functionals to approach the exchange-correlation energy (E_{xc}). This is the only unknown energetic term in this, otherwise formally exact, formalism and accounts for the electron kinetic energy difference between the exact interacting system and the non-interaction approximation, the corrections to avoid the Coulomb interactions of an electron with itself and to account for the fact that electrons are fermions and, hence, the electron density must arise from an antisymmetric N-electron wave function. Recently, Head-Gordon and coauthors[123] published a benchmark review including a total of *ca.* 200 density functionals developed in the last 30 years. Such a large number of density functionals developed to date shows the difficulty in obtaining the desired universal functional that, as postulated by the Hohenberg and Kohn theorems, should be able to describe any system of electrons interacting through the Coulomb potential and any ground state property. Note that the development of density functionals has systematically followed the best description of a particular property reducing the scope of them. Such strategy sacrifices universality by accuracy, although there have been efforts to develop new functionals describing a plethora of properties for families of systems, such as Vega-Viñes (VV) for transition metals.[124] This is the reason why one finds density functionals that provide accurate descriptions for properties like the nuclear resonance chemical shift,[125] ionization potential,[126] formation energy,[127] or electronic band gap,[128] just to name a few.

The E_{xc} term is generally divided into an exchange term (E_x) and a correlation term (E_c). The exchange term is related with the interactions between electrons with the same spin, whereas the correlation term stands for the interactions between electron with

opposite spin. Both terms are themselves functionals of the electron density. Despite the progress in the field, it is important to retain that the main source of inaccuracy in DFT is normally a result of the approximate nature of the exchange-correlation functional. Following the Jacob´s ladder proposed by Perdew and Schmidt,[129] a general viewpoint about the E_{xc} choice in the field of computational heterogeneous catalysis is described as strengths and weaknesses as follows.

The simplest form to treat E_{xc} is the local density approximation (LDA),[120] which assumes a constant electron density. Despite of the simplicity, LDA functional works rather well to describe the atomic structure of isolated molecules, small clusters, and surfaces, which constitutes a real strength.[130,131] Likewise, LDA works very well for bulk metals, where the electron density is indeed quite uniform. However, it fails when applied to study the energy related properties of molecular systems where the electron density accumulates in the bonding regions. As a consequence, LDA fails to describe the thermochemistry of simple molecules, tends to overestimate the binding energies and to underestimate lattice constants of solids. Clearly, this family of density functionals is not recommended for computational heterogeneous catalysis. Fortunately, a higher accuracy can be achieved by considering the density at each point and its gradient. This second rung of the Jacob´s ladder groups all methods that make use of the generalized gradient approximation (GGA) including PW91, PBE, RPBE, PBEsol and BLYP.[132-136] In general, GGA functionals perform better than the LDA functional when the PES becomes complex and are able to properly describe metals, a clear strength for their usage as shown in the case of H_2 chemisorption and dissociation on Cu(111).[137] For this reason, GGA functionals have been adopted broadly in computational heterogeneous catalysis due to a good balance between accuracy and computational cost.

Going upstairs in the Jacob´s ladder, one finds out the meta-GGA functionals[138] that further approximately include the Laplacian of the local electron density. This family of functionals appears to be appropriate when one wishes to compute the vacancy formation energies in metal systems.[139] The selection of meta-GGA functionals is therefore advised when vacancies play a relevant role during certain catalytic processes. Yet, GGA and meta-GGA fail to describe the electronic structure of some semiconducting and insulating systems as commented in more detail below. Above the meta-GGA, one has the family of

hybrid functionals which mixes Hartree-Fock exchange with that of the DFT functional. Hybrid functionals, B3LYP being the paradigmatic example,[140] were introduced to reach a good description of thermochemistry in molecules containing main group elements. Interestingly, B3LYP and other hybrid functionals have been broadly applied for the treatment of transition metal containing systems.[141] However, hybrid functionals are computationally expensive, especially when plane wave basis sets are employed, and have difficulties in describing correctly metallic systems, two drawbacks that make them less appropriate for computational heterogenous catalysis. In fact, GGA functionals win the balance between accuracy and computational efficiency against hybrid functionals.[124,142]

A weak point of most DFT methods, including those of the LDA, GGA, meta-GGA, and hybrid families, is the neglect of the long-range electron interactions such as dispersion that govern non-covalent bonding interactions. This results in an inadequate and sometimes erroneous description of intermolecular or molecule-surface interactions.[143] The later ones are particularly important in heterogeneous catalysis and should be included in some way. Klimes and Michaelides[144] reported a perspective article that constitutes a recommended survey about the dispersion forces and their treatment within the DFT formalism. Although with some empirical flavor, the precalculated C_6 coefficient for the dispersion energy proposed by Grimme,[145,146] leading to methods termed DFT-D2 and DFT-D3, offers a simple and yet reliable means to correct the GGA calculations at a negligible additional computational cost. On the other hand, Tkatchenko and Scheffler evaluated the dispersion correction using reference atomic C_6 coefficient, which are scaled depending on the atomic chemical environment.[147] Further improvements upon vdW-DF functionals involve changes to both exchange and non-local correlation terms that show noticeable improvements in structural and energetic calculations.[148] This set of approaches are widely employed but their need depends on the nature of investigated system. A rather recent method proposed to include dispersion is based on a Bayesian error estimation using cross-validation methods from machine learning, and has been termed BEEF-vdW.[149] The BEEF-vdW functional is competing well with GGA functionals in computing intramolecular bond energies, chemisorption energies, molecular reaction barriers, molecular reaction energies, bulk solid cohesive energies, lattice constants, and interaction energies of non-covalently

bonded complexes. Nowadays, both BEEF-vdW and PBE-D3 are becoming the most used density functionals in computational heterogeneous catalysis.

Apart from the lack of dispersion, another limitation of the standard GGA functionals derives from the intrinsic self-interaction errors,[150] which leads to an incorrect description of systems involving *d*- and *f*-electrons, *e.g.*, transition metal oxides as TiO_2, CeO_2, Fe_2O_3 or NiO, with a severe underestimation of the electronic band gap, an incorrect description of localized electrons in the reduced oxides and an equally large overestimation of magnetic coupling in those systems where such shells are partially filled.[35] These problems are partially addressed by hybrid functionals, which, however, may require larger computational resources, especially when using plane wave basis sets. A practical empirical solution consists in adding an empirical term that penalizes double occupancy of *d* or *f* orbitals,[151] with the resulting method being usually referred to as GGA+*U*. Here, the *U* parameter is often determined empirically by comparison to experiment.[152153] This type of method is needed in those heterogeneous catalytic processes where transition metal oxides are presented as active substrates like those discussed in the previous section and either the band gap needs to be described with some accuracy or where oxygen vacancies or reduced samples are involved.

By knowing the limitations and approximations inherent to the different DFT approaches, these methods can be wisely employed in computational heterogenous catalysis to analyze the PES of a catalytic reaction in a sufficiently accurate and efficient way. However, one must realize that DFT calculations do not consider temperature effects and, thus, the computed PES corresponds to 0 K. The inclusion of the temperature requires accessing standard statistical thermodynamics to estimate the Gibbs free energy at the conditions of interest. This analysis is relevant in computational heterogeneous catalysis because one may further perform realistic simulations considering the pressure and temperature conditions for a given reaction.

4. Bridging the length scales: From micro to macro

DFT allows one to access to a reasonable description of the electronic structure and thus, deals with length scales of the order of 10^{-10} meters. Moreover, the information arising from DFT calculations correspond to 0 K while the identification of the surface structure and

composition, and the corresponding catalytic activity under the reactant partial pressure (*p*) and temperature (*T*) conditions must be considered. The so-called ab initio thermodynamics formalism described below provides a simple way to take *p* and *T* into account.

Another aspect to consider when aiming at a theoretical simulation of heterogeneously catalysed reactions is the time evolution, *i.e.*, the dynamic aspects of the reaction. To this end one needs to handle the nuclear motion and this is possible by coupling DFT to classical mechanics in such a way that the forces acting on the nuclei are properly derived from the PES but where the nuclei motion is treated using the Newton equations. Depending on practical details the resulting methodology is termed Car-Parrinello molecular dynamics (CPMD) or Born-Oppenheimer molecular dynamics (BOMD).[154] A detailed description of CPMD and BOMD is out of the scope of the present work and they are mentioned here because the scales of time that can be explored cover a few ps at most, see Figure 1; recent developments regarding these techniques can be found in the recent work of Wang and Song.[155] However, the scalability of heterogeneous catalytic processes towards process engineering and production level takes place at macroscopic scale and require times scales of seconds or even longer ones, see Figure 1. Therefore, one of the main challenges is to bridge the gap between the atomistic description and the macroscopic scale based on stepwise multiscale modelling procedures that can significantly extend the length and time scales.

4.1. Consideration of p and T in computational heterogeneous catalysis

The inclusion of the effect of finite temperature and pressure requires combining DFT based calculations and concepts from statistical thermodynamics. The so-called atomistic (or *ab initio*) thermodynamics[156,157] provides a simple yet powerful framework to predict surface structure and composition as a function of *T* and *p* from electronic structure theory.[158] This formalism allows one to go beyond the information provided in the PES and to calculate appropriate thermodynamic potential functions as the Gibbs free energy for the surface at different conditions. This provides a very useful information which is particularly relevant in heterogeneous catalysis. In particular, one can easily identify the most stable surface structure and composition as a function of the environmental variables.

In the *ab initio* thermodynamics framework, one assumes that a substrate is in thermodynamic equilibrium with the surrounding gas phase, which is treated as a reservoir. Figure 3a illustrates that the CO_2 environment acts as such reservoir because it can give (or take) any amount of CO_2 to (or from) the surface without changing the temperature or pressure. To illustrate the formalism in the case of a system such as the one depicted in Figure 3a, we consider the Gibbs energy of a surface in contact with a gas at given temperature T and pressure p ($G_{surf+gas}$) and we approximate it by its DFT total energy ($E_{surf+gas}$), the Gibbs energy of the clean surface (G_{surf}) is also approximated as E_{surf} whereas that of the gas (G_{gas}) is estimated from statistical thermodynamics using the partition functions as calculated assuming an ideal gas behavior. Next, the surface free energy (γ) is defined as the difference, normalized per surface area, in Gibbs free energy between the surface-adsorbate system and its separated components. Since G_{gas} depends on T and p, it is possible to plot γ as a function of pressure (or gas chemical potential) at a given temperature and, in this way, predict phase diagrams. Using a similar reasoning it is possible to define the adsorption Gibbs energy per unit area as $\Delta G^{ad}(T,p) = \gamma_{clean} - \gamma$ where γ_{clean} is simply G_{surf} per area unit. At equilibrium, the thermodynamically stable structure minimizes the surface free energy γ (T,p) of the substrate or equivalently maximized ΔG^{ad}.

Clearly, *ab initio* thermodynamics is a powerful framework with potential applicability in heterogeneous catalysis to study the thermodynamic aspects involved in a particular process. However, the accessibility to the kinetic properties and reaction rates in the modelling of heterogeneous catalysis demands more sophisticated methods as microkinetic modelling and kinetic Monte Carlo (*kMC*).

4.2. Microkinetic modelling

The identification of the molecular mechanism behind a particular heterogeneously catalysed reaction involves exploring the PES to locate all minima defining reactants, intermediates and products, as well as all transition states connecting the minima in the PES. The knowledge of the transition states provides reliable energy barriers, whenever possible including the contribution from the zero-point energy. The search for a saddle point along the reaction coordinate for a pre-set initial and final states is not a simple task although it is

now routinely done for gas phase reactions. For reactions taking place at a surface, several transition state searching techniques have been proposed and summarised by Henkelman *et al.*[159] Different methods are adopted depending on the knowledge of the mentioned pre-set states, the nudged elastic band (*NEB*) is perhaps the most widely method whether initial and final states are used as input data.[160] The NEB method analyses a generated and relaxed string of interpolated structures between the reactant and product, called images, that attempt to approximate the minimum energy path (*MEP*) in the PES. In addition, the modified climbing image NEB (*CI-NEB*) method allows the highest energy image to move towards the energy uphill resulting on its energetic maximization along the elastic band and minimization along all other directions. However, if only the initial state is known, the dimer method is more precise.[161] Regularly, CI-NEB and dimer methods are employed synergistically, where the former provides the initial guess of the transition state, which is further refined by the latter one. Moreover, the dimer method is also the best choice when studying reactions on stepped surfaces in which the automatic generation of the NEB images is not trivial.[162,163] On the other hand, the saddle point search with the dimer method may be computationally more efficient, especially in the improved version of Hayden *et al.*[164]

Once the minima and transition state structures have been located and characterized by frequency analysis, one can readily obtain the activation energy (E_a) including the zero-point energy contribution and can make use of the vibrational frequencies to approximate the partition functions entering into the transition state theory (*TST*) expression of the rate of that particular elementary step at a given temperature as $k_{\mathrm{TST}}(T) = \frac{\mathrm{k_B}T}{h}\frac{q_{TS}}{q_R} exp\left(-\frac{E_a}{k_B T}\right)$, where q terms are the partition functions associated with the transition state (*TS*) or the reactants (*R*), which for reactions at surfaces involve vibrational degrees of freedom only. It must be pointed out that k_{TST} is formally equivalent to the Arrhenius rate constant but they differ in the associated units; k_{TST} units are s^{-1} where the units in the Arrhenius rate constants depend on the stoichiometry of the considered elementary step. This knowledge of the rates for each of elementary step in the reaction network plus the Gibbs free energy profile and thermodynamic equilibrium as a function of T and p provides useful information that can be compared to experiment, establishes the thermochemistry and

allows for further modelling of the time evolutions of the process under study by means of microkinetic modelling (*MKM*).

Within the MKM strategy, a reaction network is considered for a given catalytic reaction, which consists of a series of elementary steps. Next, the information about the reaction rates is used to formulate coupled differential equations for each elementary step which are then solved numerically for a given set of initial conditions, with further details reviewed recently by Dumesic *et al.* [165] In this way, MKM connects quantitatively molecular-level modelling with experimental data by using as inputs the outputs obtained from first-principles calculations. MKM is particularly relevant in heterogeneous catalysis because it provides a description of complex reactions by identifying key reaction intermediates and the rate-limiting step, which ultimately controls the catalytic performance.[166] The direct comparison to experiment has led to the development of several packages such as CHEMKIN, Cantera, CatMAP, MKMCXX, or Micki.[167-171]

In general, the workflow of MKM starts with the identification of all elementary steps involved in the catalytic reactions as shown for instance by Stoltze and Nørskov for the study of ammonia synthesis[172] or more recently by Gokhale *et al.*[173] for the water gas shift reaction as catalyzed by Cu. Next, DFT calculations are carried out to locate and characterize reactants, intermediates, products and transition-state energy for each elementary step. From the DFT calculations the energy and Gibbs free energy profiles are derived, the later at the condition of interest. Likewise, TST rates are obtained and the system of differential equations corresponding to the reaction network numerically solved. This solution is within the mean-field approximation since all species taking part in the reaction are considered randomly distributed with a homogeneous distribution of adsorbates, fast diffusion and static active sites.[174] However, the neglect of surface heterogeneity and of diffusion-related rate control are two aspects not considered in the microkinetic modelling that contribute to the mismatch in reaction rates between model predictions and experiments.[175] To overcome the observed drawbacks in MKM simulations, kinetic Monte Carlo simulations are required.

4.3. Kinetic Monte Carlo simulations

Monte Carlo based approaches cover many applications aiming to the resolution of complex problems by using random numbers.[176] The versatility of these approaches has made them highly popular among the Computational Chemistry and Computational Materials Science communities.[177] In this context, the kinetic Monte Carlo (kMC) method, formally attributed to Bortz *et al.*,[178] constitutes a convenient way to solve the set of coupled differential equations for a given network without having to assume a mean-field approximation.[179] This is because all possible configurations involving reactants, intermediates or products at the catalyst surface are sampled. In the kMC algorithm trajectories that propagate the system correctly from configuration to configuration are generated in such a way that the average over the entire ensemble of trajectories yields probability density functions for all states fulfilling the master equation. As in the case of MKM, a kMC simulation provides information about the time evolution of a catalytic process for which the reaction network and the rates for each elementary step are known.[180] However, as a plus over MKM, the kMC method provides additional information regarding the occupancy of the surface sites.

To understand how it works one may think about the diffusion of an isolated atom chemisorbed at a specific site on a substrate. At a certain temperature, the atom vibrates around this specific site with a certain frequency and eventually diffuses to neighboring sites with variable bond strength. To get a proper understanding of the system evolution, the time evolution must cover at least a time extent that includes several of the rare hops to neighboring sites.[181] This is not always possible with classical MD because a very long simulation may be required before one can observe one of such rare events. The kMC has the advantage of solving the state-to-state dynamics as coarse-grained hops consisting in a sequence of discrete hops from site to site, where the random selection of the sequence of states that are next visited and how long does it take for such a hop to occur follows a Markov process.[179, 182] Focusing on heterogeneous catalysis, the elementary events of adsorption, desorption, diffusion and surface reaction are simulated as instantaneous processes that happen at random times.[183] A few packages are available for carrying out such simulations as ZACROS or KMC_Lattice.[181,184]

The ideal bottom-up sequence in computational heterogeneous catalysis studies is shown in Figure 3b. It starts with the first principles calculations moving towards the

thermodynamic description at the conditions of interest and end up with suitable MKM and/or kMC simulations, this working road is directly connected with the schematic view of time and size scale depicted in Figure 1. Key selected examples of computational heterogeneous studies are reviewed below.

5. Key issues regarding CO_2 conversion and heterogeneous catalysis

There is little doubt, if any, that global warming is a real problem affecting the whole planet and that the concentration of CO_2 in the atmosphere is one of the major causes. Here, heterogeneous catalysis is called to play a key role using this greenhouse gas a raw material for production of bulk chemicals contributing at least to not increase the already too high concentration. In fact, while the U.S. emission of CO_2 per capita in 2017 (16.2 tons) is practically the same that found in 1947 (16.8 tons),[185] the cumulative CO_2 emissions, estimated from the sum of emissions produced due to burning fossil fuels and cement production, have been increasing almost exponentially (*e.g.*, 135 million tons in 1847, 9,000 million tons in 1897, 84,000 million tons in 1947, 28,4000 million tons in 1997, and 400,000 million tons in 2017).[185] Although U.S. energy-related CO_2 emissions are predicted to decrease slightly until about 2035, as a consequence of shutting-down coal-fired power plants, recent predictions point to an increase after 2035 as a result of the U.S. energy consumption growth of 0.3% per year expected from 2019 through 2050.[186] Moreover, the U.S. Energy Information Administration (EIA) projects nearly 50% increase in world energy usage by 2050, led by growth in Asia,[187] which will contribute certainly to increase the CO_2 emissions. Therefore, to reach the goal of limiting global warming, considerable efforts are still needed, and researchers have been focusing on novel stratagems for sequestration and/or chemical transformation of CO_2 into fuels or commodity chemicals.

To decrease the amount of CO_2 in the atmosphere, sequestration by means of carbon capture and storage (CCS) technologies have been proposed. These require materials that are able to capture CO_2, eventually before its separation from a flue gas mixture. Available commercial solutions for CCS involve using ionic liquids or amines, or suitable porous sorbent materials.[188] Next, transportation and subsequent release to suitable underground geologic formations is required for regenerating the sorbent. However, the global process is

quite energy intensive and economically unviable. Carbon capture and utilization (CCU) strategies, aiming at CO_2 conversion into high-value chemicals, including easily manageable and transportable liquid fuels, look more interesting since they will lead, eventually, to the so-called carbon circular economy.

In principle, high-volume chemicals can be produced from CO_2 through CCU platforms using a reaction specific heterogeneous catalyst (*cat.*). For example, CO_2 can be used in the dry reforming of methane (DRM) to produce syngas, with H_2/CO ratio of 1:1, through:

$$\mathrm{CO_2 + CH_4 \xrightarrow{cat.} 2CO + 2H_2}, \Delta H = +247\ \mathrm{kJ/mol} \qquad (1),$$

that is favored at high temperature and low pressure. The resulting CO and H_2 mixture can then be utilized for the synthesis of higher hydrocarbons through the Fischer-Tropsch process, which for production of straight-chain alkanes can be well described by the following chemical equation,

$$n\mathrm{CO} + (2n+1)\mathrm{H_2} \xrightarrow{cat.} \mathrm{C}_n\mathrm{H}_{(2n+2)} + n\mathrm{H_2O}\ (n = 1, 2, 3, \dots) \qquad (2).$$

The main problems affecting this reaction are the possible formation of carbon deposits at the catalyst surface, either from the disproportionation of CO,

$$\mathrm{2CO \xrightarrow{cat.} C + CO_2}, \Delta H = -172\ \mathrm{kJ/mol} \qquad (3),$$

or from the decomposition of methane,

$$\mathrm{CH_4 \xrightarrow{cat.} C + 2H_2}, \Delta H = +75\ \mathrm{kJ/mol} \qquad (4).$$

Methane may originate from natural gas or from potential renewable alternatives as biomass or biogas, the latter leading to effective CO_2 abatement. Besides methane, dry reforming of ethanol (DRE), from agricultural raw materials,

$$\mathrm{CO_2 + C_2H_5OH \xrightarrow{cat.} 3CO + 3H_2}, \Delta H = +297\ \mathrm{kJ/mol} \qquad (5),$$

and of glycerol, a byproduct of biodiesel production,

$$\mathrm{CO_2 + C_3H_8O_3 \xrightarrow{cat.} 4CO + 3H_2 + H_2O}, \Delta H = +292\ \mathrm{kJ/mol} \qquad (6),$$

have been suggested processes for utilization of CO_2 with concomitant positive effects in its abatement.

Renewable electricity from wind or solar farms can be used to split water into hydrogen and oxygen in an appropriate electrolyser; note, however, that strong efforts must be made in this specific area since most hydrogen is still produced from the steam methane reforming of natural gas or oil/naphta (78%) and from coal gasification (18%). The renewable hydrogen can then be combined with CO_2 to obtain high-volume chemicals. Methanol can be produced through the reverse methanol steam reforming (RMSR),

$$\mathrm{CO_2 + 3H_2 \xrightarrow{cat.} CH_3OH + H_2O}, \Delta H = -49\ \mathrm{kJ/mol} \quad (7),$$

and formic acid can be obtained through,

$$\mathrm{CO_2 + H_2 \xrightarrow{cat.} HCOOH}, \Delta H = -31\ \mathrm{kJ/mol} \quad (8).$$

Upon reaction with hydrogen, hydrocarbons can be obtained from the carbon dioxide methanation reaction, also known as the reverse steam methane reforming, methanation or Sabatier reaction,

$$\mathrm{CO_2 + 4H_2 \xrightarrow{cat.} CH_4 + 2H_2O}, \Delta H = -165\ \mathrm{kJ/mol} \quad (9),$$

or from the reverse water gas shift (RWGS) reaction,

$$\mathrm{CO_2 + H_2 \xrightarrow{cat.} CO + H_2O}, \Delta H = +41\ \mathrm{kJ/mol} \quad (10),$$

followed by subsequent hydrogenation of CO *via* the Fischer-Tropsch process, equation (3).

In addition, several reactions may benefit from the incorporation of CO_2 as an oxidant weaker than the widely employed O_2 gas. A few examples are the oxidative dehydrogenation of paraffins into olefins, exemplified below through the reaction of ethane to ethylene,

$$\mathrm{CO_2 + C_2H_6 \xrightarrow{cat.} C_2H_4 + CO + H_2O}, \Delta H = +178\ \mathrm{kJ/mol} \quad (11),$$

the oxidative coupling of methane to ethane,

$$\mathrm{CO_2 + 2CH_4 \xrightarrow{cat.} C_2H_6 + CO + H_2O}, \Delta H = +106\ \mathrm{kJ/mol} \quad (12),$$

or ethylene,

$$2CO_2 + 2CH_4 \xrightarrow{cat.} C_2H_4 + 2CO + 2H_2O, \Delta H = +284\ \text{kJ/mol} \qquad (13).$$

Some other reactions where O_2 is replaced by CO_2 are covered in the review of Tao *et al.*[189] but have been less studied (*e.g.*, olefin to epoxides) or have many associated problems (*e.g.*, alkanes to carbonyls). Note that the routes above differ from already well-established industrial reactions that combine CO_2 with petrochemically derived reagents, such as ammonia or phenol to yield urea and salicylic acid, respectively, but that do not lead to the abatement of CO_2.

6. Representative examples of computational studies for CO_2 conversion

The main problem encountered in CCU technologies (equations 1-13) arises from the very high stability of the CO_2 molecule. In fact, all processes referred above involve severe energy requirements. Therefore, suitable catalysts with long-lasting stability are needed, not only to activate the CO_2 molecule but also to selectively direct the reaction of interest towards the desired product(s) and, ideally, under mild reaction conditions. For example, the oxidative coupling of methane to ethane (eq. 12) requires catalysts that selectively activate only a single C-H of each methane molecule. Because of the enormous societal impact of CO_2, significant efforts have been undertaken to develop novel catalysts that can cope with the desiderate, considering several different kinds of materials.[190,191]

Over catalytic surfaces, one of the main routes for CO_2 activation is through coordination to a metal centre in a substrate, which is followed by substrate→CO_2 electron transfer, leading to the formation of a chemically active bent $CO_2^{\delta-}$ moiety with elongated, *i.e.*, weakened, carbon-oxygen bonds. Several different strategies for CO_2 activation by catalytic surfaces were deeply discussed by Álvarez *et al.*[192] and are outlined in Figure 4. The different strategies and different targeted reactions require specific catalysts. Therefore, significant experimental and computational efforts have been devoted to optimize existing catalysts or to develop new ones.[189-195] Hereafter, we will focus on the gas-phase thermic CO_2 conversion, and the reader is addressed to other recent reviews in cases of photocatalysis[196] and electrocatalysis.[197] Still, the literature is vast enough even when focusing on thermochemical conversion only. Thus, instead of an extensive and exhaustive description of the available literature we will comment on key paradigmatic examples

selected because of their efficiency and possible practical use and encompassing as well different employed models and computational approaches.

6.1. Single-crystal metal surfaces

Single-crystal transition metal surfaces have long been considered in catalytic studies since, as the number of active sites is limited, the understanding of catalytic reaction mechanisms is straightforward. In the specific case of the gaseous CO_2, single-crystal surfaces have been found to be less interesting since, on most metal surfaces, CO_2 simply physisorbs with a concomitant lack of activation, especially in the case of the highly stable Miller low-index surfaces. The picture is slightly different in the case of stepped surfaces or surfaces incorporating promoter species as Li, Na, or K,[198] or in the electrochemical CO_2 reduction reaction (CO2RR) where single-crystal metal electrodes, in special based on copper, have been heavily studied in the literature, both experimentally and computationally.[199,200]

Recently, Ko *et al.*[201] performed a comparative computational study of the activation of CO_2 upon adsorption on several low-index metal surfaces including Fe(110), Co(0001), Ni(111), Ru(0001), Rh(111), Pd(111), Ir(111), Pt(111), Cu(111), Ag(111), and Au(111), using the PBE density functional and adding dispersion by means of the D2 method. Noting that, this analysis corresponds to a situation where just one single CO_2 is anchored over such substrates, resulting in a low coverage situation. These authors confirmed that CO_2 physisorbs on most of these surfaces with a bent structure, except for the coinage metal surfaces, and with calculated adsorption energies between -0.22 and -0.34 eV where the minus sign indicates favourable adsorption with respect to the corresponding bare surface and gas-phase CO_2. Clear chemisorbed structures were predicted for Fe(110) and Ru(0001), with adsorption energies of -0.93 and -0.65 eV, respectively, and O-C-O angles of ~121º and ~123º, respectively. In accordance with the computed chemisorption energies, ~1.1 and ~0.8 electrons were transferred from, respectively, the Fe(110) and Ru(0001) surfaces to the CO_2 species, while in the remaining surfaces the charge transferred to the bent $CO_2^{\delta-}$ moiety was always below ~0.6 electrons. These authors also calculated the activation energies for the dissociation of CO_2 into chemisorbed CO and O species. Interestingly, the lowest activation energies were found for the Fe(110) and Co(0001) surfaces and no clear correlation between the activation energy

and the adsorption energy of CO_2 was found. Correlations were found only when plotting the activation energies against the calculated reaction energies or the sum of the adsorption energies of the products of the dissociation reaction, see Figure 3c, with R^2 values of 0.79 and 0.72, respectively, nicely following the Brønsted-Evans-Polanyi (*BEP*) earlier introduced by Neurock and Pallassana,[202] and broadly exploited by other groups.[163,203,204]

The promotor effect of potassium on the CO_2 activation was studied by Nie *et al.*[198] by comparing PBE+*U* (U_{Fe} = 3.8 eV) calculated results for the adsorption and dissociation of CO_2 on the clean and K-covered Fe(100) surfaces. These authors found that potassium prefers to adsorb at 4-fold sites rather that at top or bridge locations. The analysis of the calculated Bader[205] charges showed charge transfer from the K adatom to the Fe(100) surface. This excess charge in the K-covered surface stabilized not only the bent $CO_2^{\delta-}$ species (*i.e.*, the initial state) but also the transition (OC···O) and dissociated (CO + O) states, from -0.92, -0.12 and -2.11 eV, respectively, in the case of the Fe(100), to -1.51, -0.96, and -2.18 eV, respectively, in the case of the K/Fe(100), with the zero of energy being the separate catalyst surface and gaseous CO_2 molecule. Hence, while the reaction energy is almost unchanged, the CO_2 molecule is significantly activated by K/Fe(100) and the barrier for the C-O bond cleavage is reduced by 0.25 eV (from 0.8 to 0.55 eV) upon addition of K.[198]

Lozano-Reis *et al.*[206] carried out a complete study to investigate the molecular mechanism of CO_2 hydrogenation on Ni(111); the motivation being the high activity demonstrated by Ni-based catalysts for this reaction. They carried out calculations with the BEEF-vdW density functional followed by kMC simulation considering a reaction network encompassing the global reactions described by eqs. 7, 9, and 10 above, totalizing 25 different species (6 gaseous reactants/products and 19 adsorbed intermediates) and 86 elementary processes, including adsorptions, desorptions, surface chemical steps and diffusions. The kMC involved a lattice model where each point corresponds to sites at the Ni(111) surface (*i.e.*, fcc, hcp, bridge, or top). The steady-state coverages of the main surface species at pressures of 1 and 10 bar and temperatures of 573.15 and 673.15 K, which are typical Sabatier reaction conditions are provided in Table 1. As it can be seen, the surface coverage by the considered intermediate species is below 1%, with the exception of hydrogen adatoms that, depending on the reaction conditions, varies between 7

and 17%. These low values are the result of the too weak adsorption energies calculated for the reactants, intermediates and products on the Ni(111) surface. Since according to the Le Sabatier principle catalyst surfaces presenting too weak or too strong interactions with the adsorbates exhibit low activity, the extended Ni(111) surface is expected to be weakly active towards the CO_2 hydrogenation. In fact, the turnover frequencies (*TOF*) calculated by Lozano-Reis *et al*.[206] were all very low, which clearly suggest that the activity towards the RWGS and Sabatier reactions of Ni-based catalysts observed experimentally is due to Ni species with a rather different nature of the high-coordinated atoms on the extended (111) facets. Thus, the activity may be attributed to low coordinated atoms, either in corrugated surfaces or in particles deposited onto a support, without excluding possible synergic effects at the particle/support interface (see below).

6.2. Free standing and supported metallic nanoparticles

Metallic (nano)particles, usually deposited onto a substrate, have been shown to have enormous potential for catalytic reactions because of the presence of significant amounts of undercoordinated metal atoms while minimizing the amount of bulk metal atoms not participating in catalytic processes. The sizes of the metal particles can be changed to obtain different proportions of atoms with varied atomic environments, hence, having different reactivities. The preparation of catalysts with metal particles dispersed onto a substrate is nowadays carried out in a routine way[207] but recent developments have succeeded in controlling the size of the supported particles[208,209] to reach the single atom catalyst limit.[210] For example, recent CO_2 activation studies reported the preparation of Ni SAC deposited or embedded on different substrates,[211-214] and of Ni particles with sizes from 1 to 10 nm deposited onto a SiO_2 substrate.[215] Ni@MgO SAC were considered for the RWGS reaction (eq. 10) and found to be 100% selective towards CO at temperatures below 300 K; DFT calculations supported the correlation between activity and amount of exposed Ni atoms attached to low-coordinated sites in the oxide support.[214] Curiously, as the temperature increases, Ni clusters were found to form and methane appeared as a product of the reaction. The rather different catalytic properties of Ni@MgO SAC and tiny Ni clusters at MgO are very well rationalized in a separate DFT/kMC study by Zuo *et al*.[216] These authors compared the activities of MgO(100), Ni_1@MgO(100) and Ni_4@MgO(100) catalysts towards the DRM (eq. 1) and found that while Ni improves the binding properties

of MgO, one Ni atom is not enough to dissociate CO_2 and CH_4. In fact, while CO_2 is highly bent (133.5^o) when adsorbed on the bare MgO(100) surface, the reaction is highly endothermic (3.95 eV) because the products of its dissociation interact weakly with the catalyst surface. The same applied to methane which interacts very weakly with the MgO(100) surface (E_{ads} = -0.04 eV). On the SAC, the adsorption energies of the products of reaction increase but that of CO_2 decreased (the reaction became slightly less endothermic, 3.62 eV) and the barrier for the $CH_4 \rightarrow CH_3 + H$ was still very high (1.57 eV). In the case of the Ni_4@MgO(100) catalyst model, CO_2 adsorbed strongly (-0.99 eV) and the barrier for the dissociation becomes 0.35 eV only, and lower than that calculated on the extended Ni(111) surface (0.42 eV). Importantly, the quite small size of the Ni particle was found to be important to hinder the formation of C adatoms through $CO \rightarrow C + O$ because of the site confinement. The adsorption of methane was found to be more favorable on Ni_4@MgO(100), E_{ads}=-0.17 eV, than on MgO(100) and Ni_1@MgO(100) and the barriers for methane dehydrogenation were calculated as 0.53, 0.55, 0.38 and 1.06 eV for $CH_4 \rightarrow CH_3 + H$, $CH_3 \rightarrow CH_2 + H$, $CH_2 \rightarrow CH + H$ and $CH \rightarrow C + H$ steps, respectively. Thus, coke formation is unlikely and, even when C adatoms are formed, these species will be oxidized to CO through a calculated barrier of 0.56 eV only, significantly lower than the barrier associated with the last dehydrogenation step above. The DFT energies were used to feed a kMC study although diffusion barriers were neglected. This study assumed that the MgO substrate is too inert to participate in the reaction, which is supported by the DFT data, and that the DRM reaction is confined to occur at Ni triangle sites of the Ni_4 cluster, without diffusion of adsorbates from one cluster to another. The kMC simulations confirmed the absence of coke formation and that the conversion and selectivity to H_2 increase with the temperature.

The role of the support in the CO_2 activation by nickel-based catalysts was deeply investigated by Silaghi *et al.*[217] upon comparison of CO_2 adsorption and dissociation on Ni(111) and stepped Ni(211) surfaces and on Ni_{13} or Ni_{55} particles, either bare or deposited onto (100) or (110) terminations of the γ-Al_2O_3 support. The results of their DFT based calculations with the PW91 density functional clearly suggest that for the unsupported Ni system, the CO_2 adsorption strength and reactivity increases from Ni(111), to Ni(211), to Ni_{55}, and to Ni_{13}, which is clearly related with the decrease of the coordination number of

the exposed Ni atoms. They also found that the CO_2 binding energies on the Ni_{13}@ γ-Al_2O_3 and Ni_{55}@ γ-Al_2O_3 systems was significantly higher than on the bare nanoparticles, which shows the synergic effects of the support in enhancing the charge transfer to the adsorbed CO_2 species. Importantly, they found also that most reactive system was Ni_{55}@ γ-Al_2O_3(110) in which the CO_2 activation occurs at the interface between the metal particle and the support. The support not only stabilizes the cleaved O adatom but also allows to an increased separation of the CO and O fragments in the CO···O transition state. The importance of the support in the CO_2 activation is also evident on Pt-based catalyst models. Kattel *et al.*[218] used the same density functional to study CO_2 hydrogenation on Pt_{46}, Pt_{25}@SiO_2 and Pt_{25}@O_{vac}-TiO_2 systems and found that, while the bare nanoparticle is not able to catalyze the reaction due to weak CO_2 binding, the hydrogenation towards methane progresses well on the supported Pt nanoparticles through RWGS and CO hydrogenation steps. As in the study of Silaghi *et al.*[217] the sites at the Pt–oxide interface plays an important role in enhancing the catalytic activity. Thus, summing up, the inferior activity of pure metal catalysts towards the activation of CO_2 are aligned with the conclusions from Lozano-Reis *et al.*[206] described earlier.

6.3. Transition Metal Carbides

Transition Metal Carbides (*TMCs*), typically involving early transition metals, have emerged as promising materials for CO_2 conversion. These materials are normally regarded as available and economic potential substitutes to catalysts based on scarce and expensive Pt-group late transition metals, displaying similar or even superior catalytic activities and selectivities.[219] One appealing aspect of TMCs concerning CO_2 conversion is that such materials display significantly strong CO_2 adsorption energies,[220] *e.g.*, ranging from -0.61 eV for the C-terminated orthorhombic β-Mo_2C (001) surface, to -3.27 eV for Mo-terminated β-Mo_2C (001) surface,[221] as estimated by DFT means using slab supercell models and the PBE density functional.[133] Regardless of the TMC crystal structure, a common feature is that CO_2 gets not only strongly adsorbed, but also significantly activated; this is, with a bent geometry, see Figure 5a, and displaying a negative Bader charge.[205]

Indeed, TMCs have been investigated as CO_2 capture and storage materials for a large diversity of conditions,[222] including CO_2 at air partial pressure, from exhaust gases, and even at standard conditions of 1 bar, upon comparison of computationally estimated rates of adsorption and desorption. The proper CO_2 capture and activation are indeed critical for the possible CO_2 conversion catalysed by these materials,[223] either directly to CO, *e.g.*, through the RWGS reaction (eq. 10) or to methanol through the RMSR reaction (eq. 7). Notice that the similar structure of Transition Metal Nitrides (*TMNs*) also points for their possible usage, yet so far less studied, with the accent put on the CO_2 electroreduction.[224]

As far as CO_2 conversion on TMCs is concerned, one particular aspect to be regarded is the possible formation of O adatoms, eventually leading to the formation of oxycarbides.[225] These have long been considered as inactive, and oxycarbide formation seen as a catalyst deactivation mechanism, killing the surface chemical activity. This has been observed, for instance, in the weakening of CO_2 adsorption on the β-Mo_2C(001) surface upon increasing O adatom coverage[226] with a concomitant overall effect on all the reaction energy path.[227] This is the reason why the redox mechanism of the water gas shift (WGS) reaction should be avoided when using a TMC-based catalyst.[227,229] However, recent studies point out a change of paradigm, as oxycarbides surface models, particularly of group IV transition metals, were found to strengthen the CO_2 adsorption and activation.[230]

Aside from the previous considerations, it is worth to mention that theoretical calculations have shown that the surface chemical activity of TMCs towards CO_2 can be tuned on/off through different fashions; for instance, by doping the TMC surface so as to have surface doped single atom catalysts. These special sites have been predicted to tune the CO_2 capturing capabilities while maintaining the CO_2 activated mode.[231,232] Although practical realization of this idea remains to be done, although such a strategy has been used to improve the electrochemical reduction of CO_2 towards CH_4 on TiC and TiN surfaces.[233] Another way of fine-tuning catalytic active centres towards CO_2 is the generation of surface vacancies. These are intrinsically present in V_8C_7 and calculations for a (001) surface model reveal the key role played by these vacancy active sites, not only changing the

preferred RWGS mechanism from redox to associative when compared to the defect-free VC(001) surface, but also reducing the rate limiting step energy barrier for almost 1 eV.[74]

Still with the RWGS reaction, it is worth highlighting the prominent performance of molybdenum carbide-based catalysts. For instance, hexagonal α-Mo_2C nanoparticle catalysts are able to reach the thermodynamic maximum CO_2 conversion of 16% and a selectivity towards CO above 99% at the 673 K working temperature.[89] Density functional calculations carried out to investigate the structure a α-Mo_2C NP by means of the Wulff analysis revealed that polar Mo- or C-terminated (001) surface, plus non-polar (101) and (201) surfaces accounted for *ca.* 84% of the exposed surface under working conditions.[234] Indeed, the theoretical modelling and calculated reaction free energy profile at 600 K with equal pressures of 0.2 bar of both CO_2 and H_2 reactants, see Figure 5b, revealed that all surfaces are well capable of adsorbing, activating, and easily breaking CO_2, with energy barriers below 0.59 eV, and specially low for Mo-terminated surfaces, in line with previous results on tungsten carbides with barriers as low as 0.71 eV for W-terminated surfaces.[220] Similarly, H_2 easily dissociates on all the explored TMCs[220,235] indicating that they may be useful for CO_2 conversion to methanol, formic acid, or CO in an H-assisted mechanism.

An important aspect of the study commented above is that it reveals that, counter-intuitively, the sites at (001)-Mo and (201) sites, exhibiting the lowest energy barriers for the CO_2 dissociation, are not the responsible for the experimentally observed reactivity. The reason is that their low energy barriers are due to the stronger stabilization of the reaction step products, following the BEP relationship[202-204] correlating energy barriers and reaction step energies, in such a way that the more exothermic the reaction step energy, the smaller the barrier. In the case of catalytic CO_2 conversion by α-Mo_2C, the drawback is that the products reach a thermodynamic sink so that their desorption becomes too difficult and the catalyst becomes poisoned. In this sense, the (001)-C surface, and specially, the (101) surface reveal larger energy barriers of 0.59 and 0.57 eV, respectively, but the reaction products are just 0.59 and 0.21 eV away from products. Indeed, the (101) surface is the catalytically most suited surface, a point that coincides in the increasing catalytic activity while increasing the temperature, and the increasing exposure of (101) surfaces with temperature.[234] This example shows the need to investigate in detail all aspects before

reaching conclusions that may prove to be incorrect simply because only a part of the history has been disclosed.

Apart from the direct use of TMCs as catalysts, these materials exhibit very interesting properties as supports of metallic particles either for heterogeneous catalysis or electrocatalysis. Precisely, WC nanoparticles coated with transition metals have been appointed as efficient electrocatalysts for CO_2 methanation and the RWGS.[236,237] Likewise, TMC have been used as supports for small metallic clusters with experimental evidence of an increased activity when compared with the same metal on other supports.[238] This important effect has been attributed to the TMC support polarization of the electron density of the supported metal atoms or clusters.[239 - 241] The effect of this polarization is unexpectedly large, resulting in significantly enhanced catalytic activities and tuned selectivities in desulfurization reactions,[242,243] the WGS reaction,[244] and the RWGS and methanol formation reactions.[245]

More recently, experiments have shown that the noticeable reactivity of the rock-salt δ-MoC(001) surface is tremendously enhanced when small Cu clusters are deposited onto it. The experiments show a great improvement in the generation of both CO and methanol in Cu/δ-MoC compared to δ-MoC. Here, theoretical calculations explained the molecular mechanism that is found to proceed through the RWGS without CO_2 methanation.[246] More in detail, the computed PBE Gibbs free energy profiles at the working conditions, generated by using slab models with the supported Cu_4 clusters, reveal a distinct reactivity for the supported Cu_4 clusters compared to the bare δ-MoC(001) surfaces, see Figure 6. From the Gibbs free energy plots it becomes clear that on the δ-MoC(001) surface the associative mechanism of the RWGS is preferred over the direct CO_2 dissociation, with Gibbs free energy barriers of 0.78 and 1.41 eV, respectively.

Indeed, methanol formation is hindered in the posterior step of CH_3O* formation, featuring a Gibbs free energy barrier of 0.86 eV. However, for the system with supported Cu_4 clusters, the associative mechanism becomes blocked because of a prohibitive COOH formation Gibbs free energy barrier of 1.29 eV. On the other hand, the direct CO formation is greatly enhanced, with a Gibbs free energy barrier of 0.65 eV only. Indeed, methanol synthesis is also favoured when considering a bifunctional catalyst, where different parts of the reaction are carried out on different regions of the catalysts. Thus, assuming a suitable

flux of species between the Cu_4 cluster and the support region, well possible because the diffusion energy barriers are almost always smaller than the reaction ones,[247] the model catalyst study fully explains the observed experimental values of CO and methanol production increments, plus unfolding changes in the preferred reaction mechanisms.

6.4. MXenes

The so-called MXene materials, discovered in 2011,[248] are few-layered transition metal carbide or nitride materials and, in this way, constitute bi-dimensional (2D) versions of rock-salt TMCs and TMNs. The 2D nature of the materials is precisely the reason to name them is such a way that it is reminiscent of graphene.[249] MXenes have normally a $M_{n+1}X_n$ stoichiometry, where M is typically an early TM, X = C or N, and n = 1-3, although MXenes with n = 4 have been isolated recently.[250] These materials are obtained from MAX phases, where the A component, gluing the MXene patches, is usually a *p*-block element. In the MXenes synthesis, the A element is selectively extracted benefitting from a weaker M-A bond compared to M-X. The most regular procedure is the A extraction using hydrofluoric acid (HF) or *in situ* generated HF,[248,251] followed by a sonication step to separate the MXene layers. This typically leaves the MXenes as $M_{n+1}X_nT_x$, where T_x is the termination of their M surfaces, being composed of a mixture of –O, -OH, -F, and –H groups. However, annealing and hydrogenation procedures have been reported to generate pristine MXenes.[252] Very recently other procedures have emerged to obtain other halide based MAX phases from which one can directly isolate pristine MXenes.[253] It is also worth pointing out that the MXene family is vaster than expected, with the possibility of having carbonitrides,[254] as well as of having alloys within a metal layer, the so-called inner-MXenes or i-MXenes, or different stacked metal layers, in the so-called o-MXenes.[255] MXene materials have been mostly proposed for energy conversion and storage applications as in supercapacitators and substrates for Li-based batteries.[256] However, their use in catalysis has been gaining momentum,[257] where photo- and electrocatalysis have risen as most prominent and studied fields.[258,259]

Regarding the possible use of MXenes as catalysts for CO_2 heterogeneous conversion is concerned two features are to be highlighted when comparing to bulk rock-salt TMCs and TMNs. On one hand, their 2D structure provides high-surface effective areas, up to above 300 $m^2 \cdot g^{-1}$, which are *ca.* one order of magnitude superior to those of

typical TMC NPs. On the other hand, the MXenes basal (0001) planes are equivalent to TMCs and TMNs polar (111) surfaces, which normally display surface energies much higher than those of the (001) non-polar surfaces and, consequently, are rarely exposed.[260,261] Indeed, the high surface energy, seized, for instance, by the exfoliation energy, is linked to a high chemical activity,[262] indicating that MXenes may be active enough to catalyse bond breaking on highly stable molecules. This has indeed been predicted for N_2 dissociation and ammonia synthesis.[263,264]

The high chemical activity of MXenes is evidenced in theoretical prediction for CO_2 capture. Recent density functional calculations with the PBE-D3 method carried out to investigate the interaction of CO_2 with pristine slab models of M_2C MXenes revealed quite strong adsorption energies ranging from -1.13 (W_2C) to -3.69 eV (Ti_2C), which suggest that they may be used in CCS technologies for CO_2 abatement. This is supported by comparing estimates of the adsorption and desorption rates as a function of CO_2 partial pressure and working temperature extracted from collision theory and TST, respectively.[265] Interestingly, the theoretical predictions have been later experimentally confirmed, with CO_2 uptakes larger than the theoretical conservative estimates.[252] Actually, the distinctive CO_2 and CH_4 adsorption energies on M_2C MXenes has been pointed out as a way of using such materials for an ultra-highly effective biogas upgrading.[266] Moreover, the CO_2 capturing capabilities were found to change very little with the MXenes width.[267] Importantly, similar adsorption properties have been appointed for M_2N MXenes.[268]

The CO_2 adsorption and desorption calculated rates as a function of the CO_2 partial pressure, p_{CO_2}, and the system temperature can be used to build kinetic phase diagrams, which outline a map of CO_2 capture conditions. The adsorptive modes of CO_2 feature a bent geometry, with elongated C-O bonds, and a partial negative charge, as seen in Figure 7. This figure also shows that both bulk HfC(111) and $Hf_{n+1}C_n$ MXenes (0001) surfaces exhibit a larger area for CO_2 capture — broader set of conditions— than HfC(001) surfaces. Both HfC(111) and $Hf_{n+1}C_n$ MXenes (0001) are predicted to be good candidates for CO_2 abatement at normal conditions of temperatures for even very low p_{CO_2}.

The intrinsic properties discussed above make MXenes very appealing materials for CO_2 conversion, although the literature so far just succinctly grazed this possibility, and mostly from the electrocatalytic point of view through the CO_2 reduction reaction, for

instance, found to be selective towards CH_4 in the so called CO_2 methanation, as shown for M_2C and M_3C_2 types of MXenes.[269,270] However, such studies electrocatalytic studies lack a kinetic treatment by analysing the reaction steps energy barriers, with only few examples, *e.g.*, the easy CO_2 hydrogenation into OCOH on Cr_3C_2 with an energy barrier of 0.38 eV.[270] In any case, energy barriers can be key in any process, and a significant scientific advance has been recently disclosed in what concerns the catalytic dry reforming of methane. In this reaction, the CO_2 first C-O bond dissociation is regarded as the key rate limiting step but this appears to be easily achieved on a partially O-covered Mo_2C MXene, with an estimated Gibbs energy barrier of solely 0.3 eV, see Figure 8.[271] This is very much in line with the CO_2 dissociation energy barriers of 0.21 and 0.17 eV for β-Mo_2C and α-Mo_2C Mo-terminated (0001) or (001) surfaces, respectively, as both display a very similar hexagonal close-packed layer of surface Mo atoms.[89,272] Indeed, CO_2 is no longer involved in the rate limiting step, which corresponds to the CH_4 first C-H bond scission with an energy barrier of ca. 2.35 eV, as a result of the little interaction of CH_4 with the MXene, and the high stability of CH_4, see Figure 8.

7. Concluding remarks and outlook

Catalysis is pivotal to advance in solving the energy and environmental crisis and, thus, highly efficient catalysts for the generation and storage of fuels are needed. The challenge is huge and research advances from all possible sides have to be invoked. In this review, we have presented and discussed the state-of-the-art modelling and computational techniques including also some historical hints, which, we believe, contribute to have a better perspective on the present status of the field. The power and limitations of the different models and methods have been illustrated taking the heterogeneously catalysed conversion of CO_2 as case of study. The importance of using realistic models coupled to sufficiently accurate computational methods is highlighted as a prerequisite to provide reliable results that can be directly compared to experiments. This is no doubt one of the key challenges to contribute to catalysis by design. Linking catalytic performance to the properties of the catalyst and how the surface electronic structure determines somehow the resulting catalytic properties is fundamental to understand industrial catalytic processes under *operando* conditions as smartly explained by Nørskov et al.[109]

An important challenge in modern heterogeneous catalysis is to shed light on the nature of the active sites and to understand how their structures evolve when exposed to the realistic catalytic environments and temperatures. The computational approaches discussed here go from DFT modelling of the reaction mechanism to thermodynamic predictions on the equilibrium state of the catalyst at working conditions and, finally, the microkinetic and/or kinetic Monte Carlo simulations that are able to make a prediction of the total turnover frequency under practical conditions, either in laboratory or in industry. The sets of models and methods available provide a way to comprehensively sample the complex chemical space, to provide suitable candidates for the potential active site, to assess the thermodynamic stabilities as a function of the reaction conditions and to simulate the whole catalytic cycle.

The advent of the digital era allowed big data management, and machine learning techniques are now at hand to screen materials in a powerful way. Initiatives such as the materials project,[273] NOMAD,[274] and Catalysis-Hub[275] are likely to play an increasing role in the future. These new approaches will, and already have, contribute(d) to advance, and shape the field of heterogeneous catalysis. In particular, machine learning can be used in concert with DFT modelling to provide the necessary predictive mechanism that effectively enables the transition from the theoretical modelling to theoretical-guided catalyst design.[276] However, even if machine learning can speed-up materials discovery, the need to understand and to rationalize the predictions remain and the feedback between these computational approaches is expected to facilitate catalyst discovery. In addition, the present databases are far from being representative of the vast number of systems encountered in practical heterogeneous catalysis as they are nurtured from the systems that have been considered hot by the computational heterogeneous catalysis community. Hence, more material models —ideally including reactants, intermediates, and products— need to be included to fully implement these new tools in heterogeneous catalysis research. Indeed, we need further data beyond ideal surfaces. Thus, realistic catalysts designed by facet engineering are demanded. This will help to bridge the gap bet between simplified descriptors-based bulk materials screening and detailed mechanistic/kinetic studies, ideally by developing meaningful surface descriptors.[277]

From a computational viewpoint, we would like to stress the need that authors report reaction mechanisms and the associated relevant data following the FAIR Data Principles that have been proposed to make data findable, accessible, interoperable and reusable.[278] This will allow meaningful and consistent comparison between different substrates. The need to carefully study the previous literature cannot be disregarded. Both aspects are intimately related and need to be promoted to reach optimum practices in computational heterogeneous catalysis.

Acknowledgments

This work was supported by the Spanish MICIUN/FEDER RTI2018-095460-B-I00 and *María de Maeztu* MDM-2017-0767 grants and, in part, by *Generalitat de Catalunya* 2017SGR13 grant, and COST Action CA18234. AM-G thanks the Spanish MICIUN for his *Juan de la Cierva* (IJCI-2017-31979) postdoctoral research contract. JRBG thanks *Fundação para a Ciência e a Tecnologia* (FCT/MCTES) and the European Regional Development Fund (FEDER), under the PT2020 Partnership Agreement, for project CICECO-Aveiro Institute of Materials, Refs. UIDB/50011/2020 and UIDP/50011/2020, and Program Investigador FCT. FI acknowledges additional support through the 2015 ICREA Academia award for excellence in University Research.

Table 1. Steady state coverages of some species during the CO_2 hydrogenation on the Ni(111) surface from the kMC simulations reported in Ref. 206.

	T = 573.15 K		T = 673.15 K	
Coverage (θ)	$p(H_2)$ = 0.8 bar $p(CO_2)$ = 0.2 bar	$p(H_2)$ = 8 bar $p(CO_2)$ = 2 bar	$p(H_2)$ = 0.8 bar $p(CO_2)$ = 0.2 bar	$p(H_2)$ = 8 bar $p(CO_2)$ = 2 bar
θ(H)	12.69 ± 0.08	17.33 ± 0.06	7.69 ± 0.06	12.36 ± 0.09
θ(CO)	0.031 ± 0.004	0.140 ± 0.019	0.007 ± 0.003	0.020 ± 0.004
θ(O)	0.170 ± 0.011	0.227 ± 0.011	0.675 ± 0.028	0.810 ± 0.024
$\theta(CO_2)$	0.769 ± 0.008	0.926 ± 0.018	0.695 ± 0.011	0.775 ± 0.023
θ(OH)	0.007 ± 0.004	0.023 ± 0.006	0.055 ± 0.004	0.076 ± 0.004

Figure 1 Schematic view of time and size scales, and typical regions of applicability of different computational chemistry methods. Images nearby regions show atomic model examples.

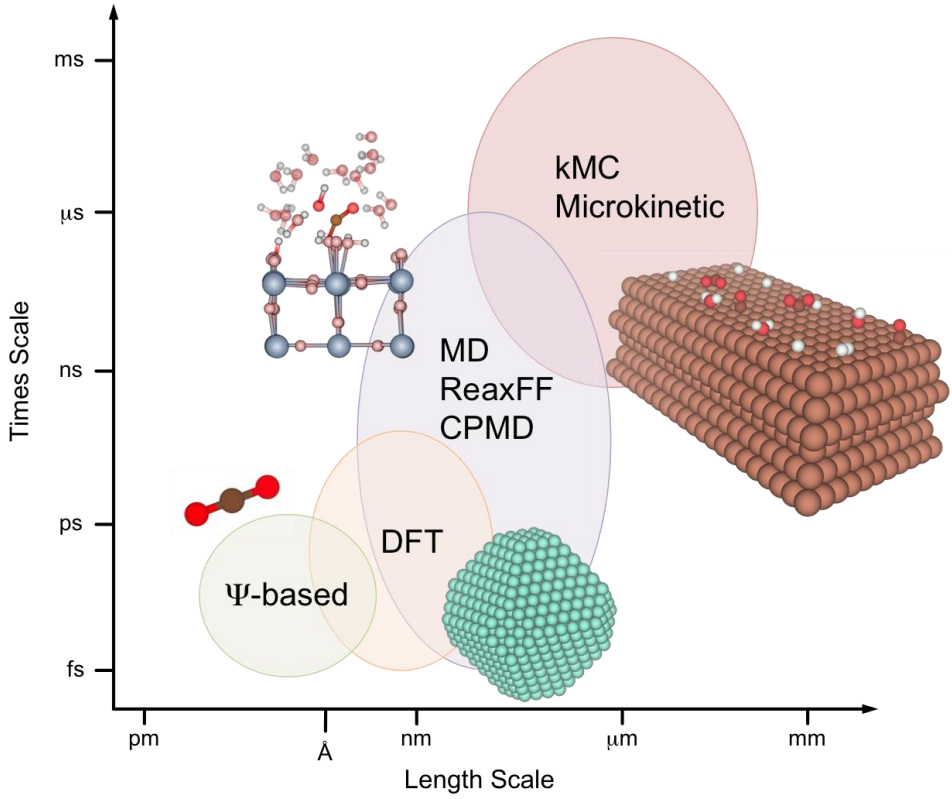

Figure 2 (a) Schematic view of metal NP (grey spheres) supported on a rock-salt oxide surface (light and blue spheres). Notice how the substrate surface features terraces and steps, with defects. Nearby images represent different models used to represent different parts of the whole system, including cluster models (brown spheres), nanocrystallites (green spheres), cluster models showing substrate defects (orange and dark blue spheres), regular surface slab models (yellow and cyan spheres), and vicinal surfaces (pink and violet spheres). (b) Schematic representation of a given property evolution with size, here denoted as metal cluster and NP models of increasing size, revealing the oscillation of the property value with size in the non-scalable region, and the linear evolution towards the bulk from the scalable region onwards.

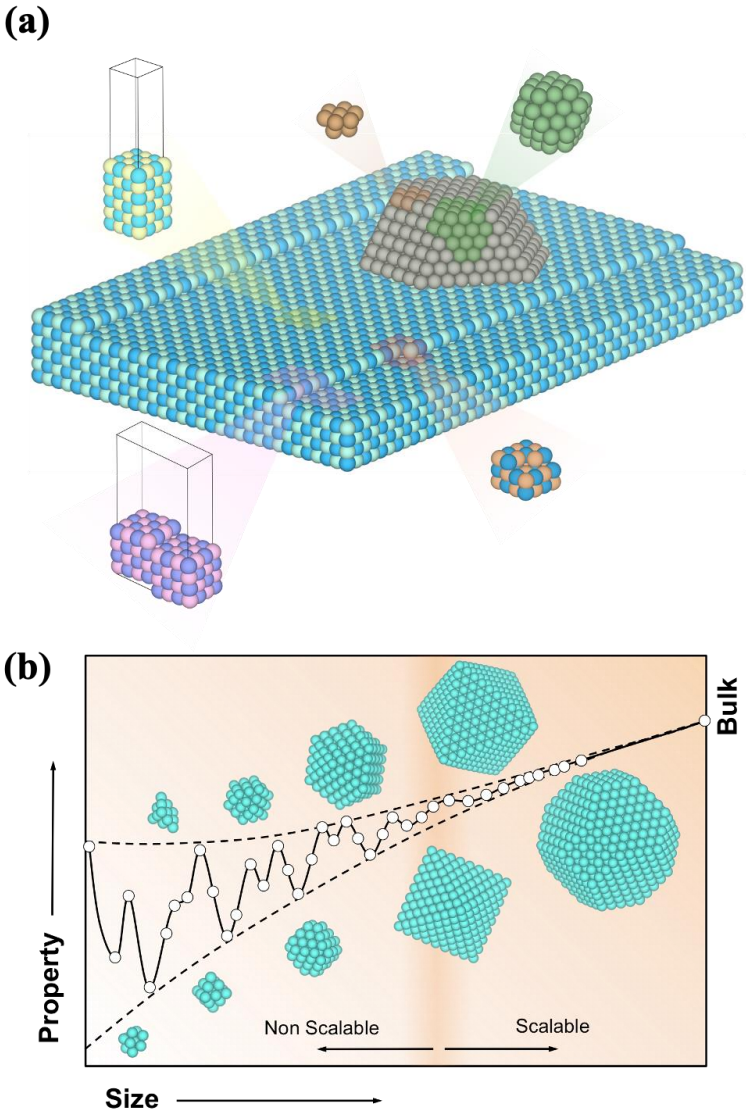

Figure 3 (a) Scheme of a solid surface in contact with the surrounding CO_2 gas phase characterized by defined *T* and *p*. Generic free energy plot for a surface in equilibrium with a surrounding CO_2 gas phase. (b) Schematic representation of the bottom-up computational strategy that aims to propagate the predictive power of first-principles techniques up to increasing length and time scales providing insights into the ongoing surface chemistry over a wide range of temperature and pressure conditions. (c) Brønsted-Evans-Polanyi (BEP) relationships between the activation energy for CO_2 dissociation into chemisorbed CO and O species on several low-index transition metal surfaces and the reaction energy (left panel) or the sum of the adsorption energies of the products of the dissociation reaction (right panel). Graphs made with data from Ref. 201.

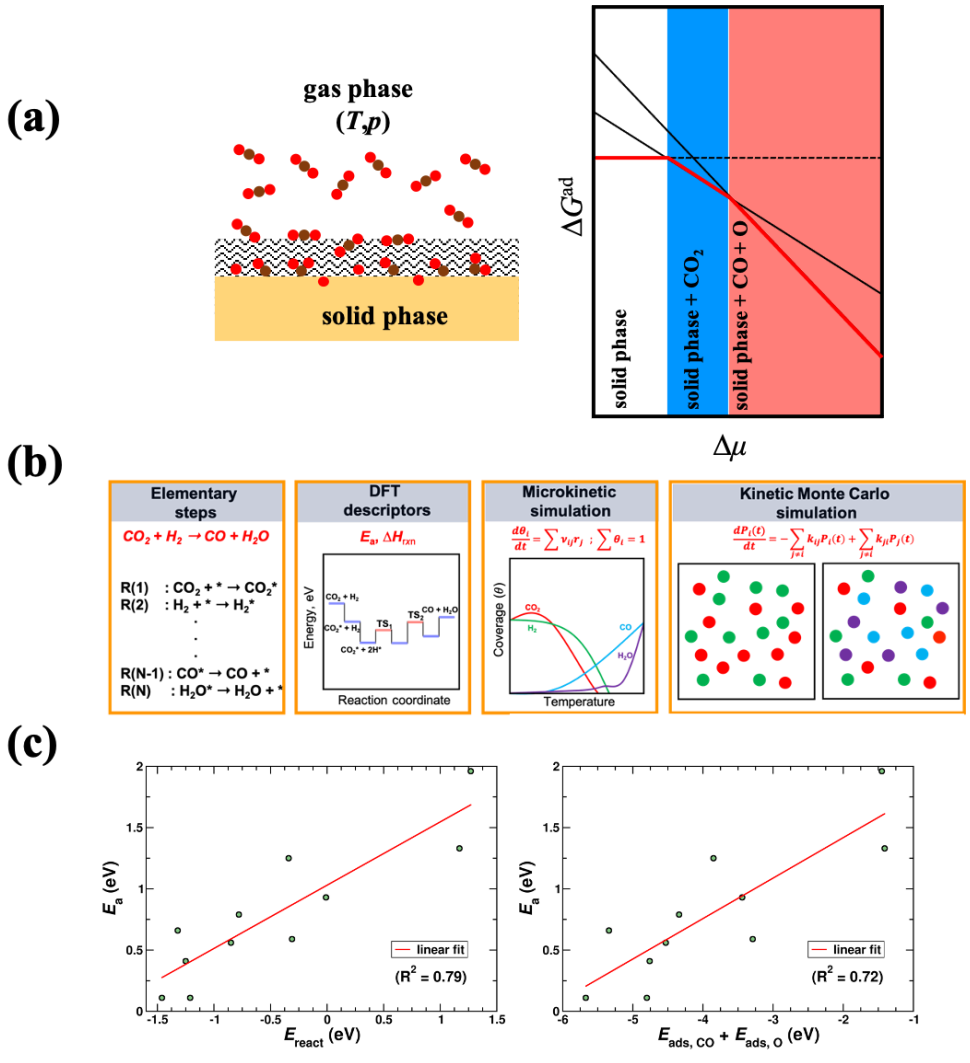

Figure 4 Different pathways to activate CO_2 over catalytic surfaces upon substrate→CO_2 electron transfer to form an active bent $CO_2^{\delta-}$ moiety. Reprinted with permission from ref. 192.

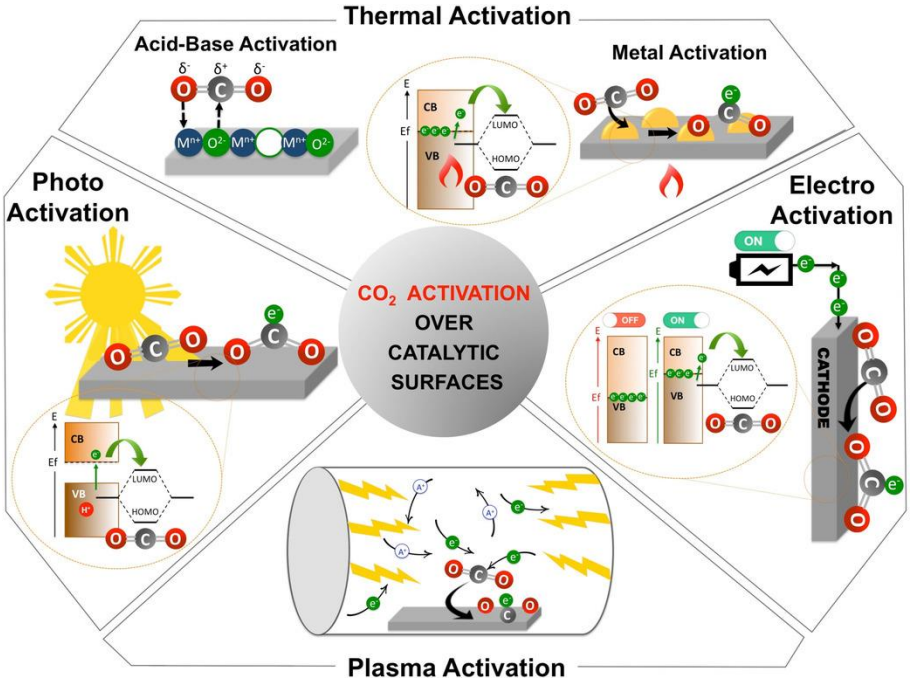

Figure 5 (a)Top (top) and side (bottom) views of activated, bent CO_2, adsorbed on a six-layered, 3 relaxed +3 fixed, (2√2×2√2)R45º TiC(001) slab model, either on a TopC (left) or an MMC (right) conformation. Carbon, Oxygen, and Titanium atoms are shown as brown, red, and blue spheres, respectively. Notice that fixed layers are shown in light colours. (b) Gibbs free energy surfaces of the CO_2 dissociation to CO+O from most stable sites on different α-Mo_2C surfaces at the working conditions of T = 600 K, p_{H_2} = p_{CO_2} = 0.2 bar, p_{CO}= p_{H_2O} = 1 mbar. Based on the data from Ref. 89.

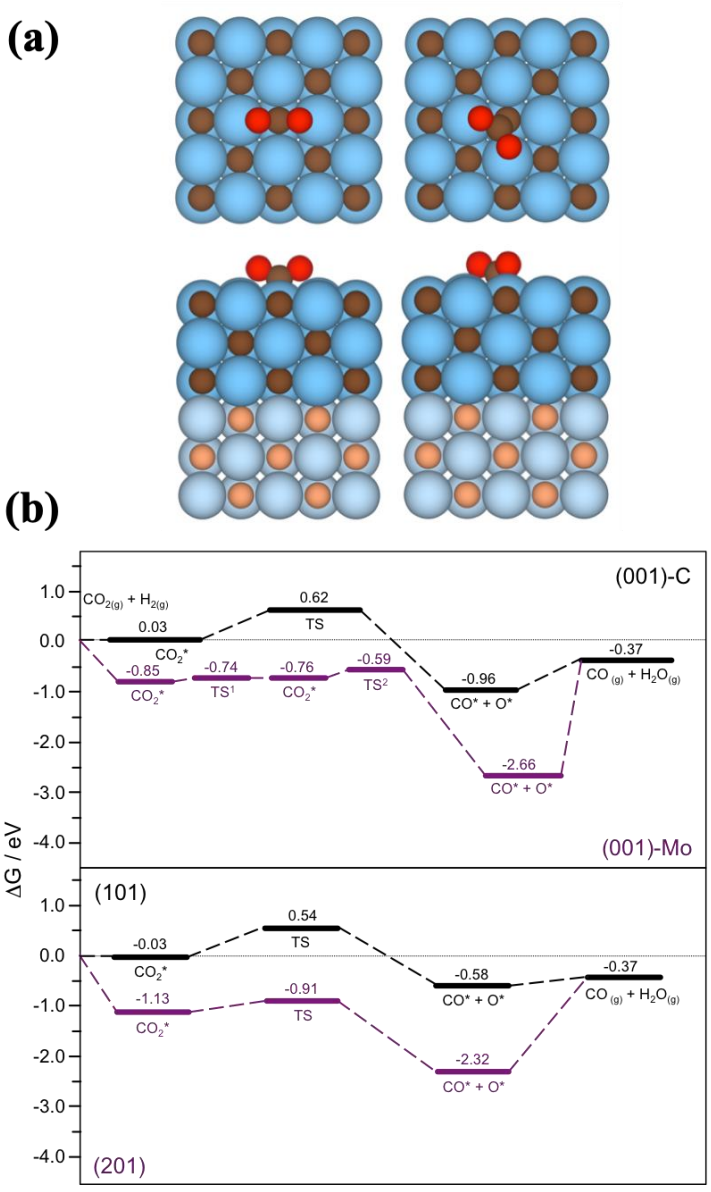

Figure 6 Gibbs free energy barriers, in eV, and side atomic views for different reaction steps through the COOH formation or the direct CO_2 dissociation and posterior CO successive hydrogenations towards CH_3OH, as computed on the Cu_4@δ-MoC(001) (left) and δ-MoC(001) (right) surface models. Based on the data from Ref. 246. Mo, C, Cu, O, and H atoms are shown as violet, green, orange, red, and white spheres, respectively.

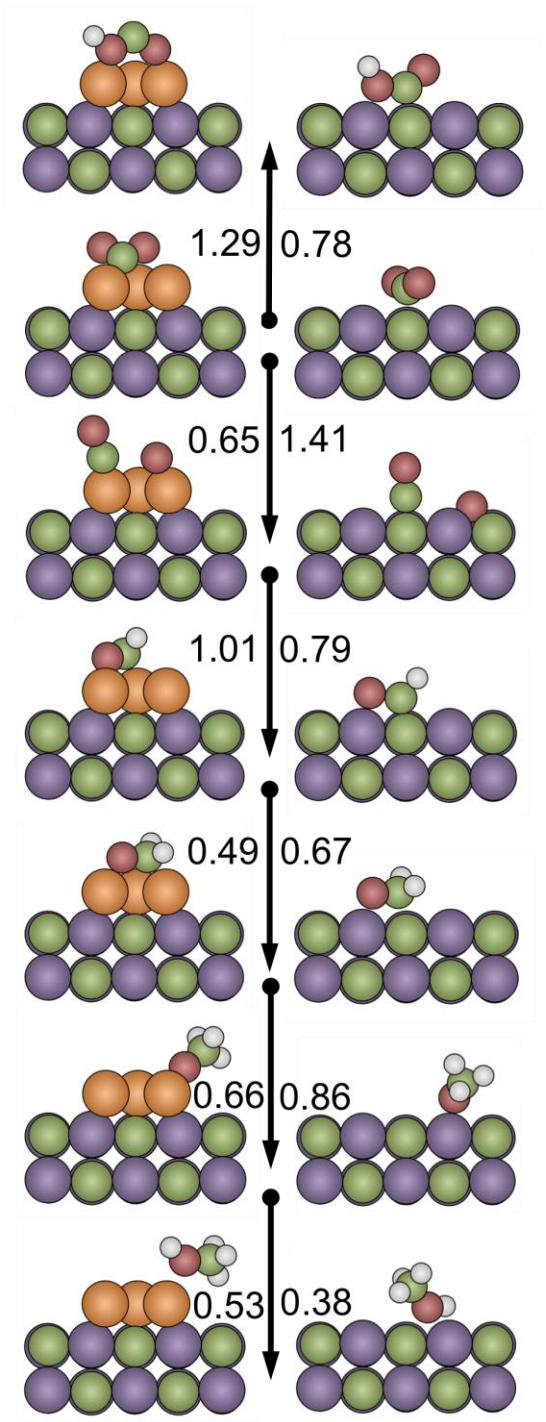

Figure 7 Kinetic phase diagram (top) for $Hf_{n+1}C_n$ MXene (0001) surfaces with results for HfC(001) and HfC(111) surfaces included for comparison. White dashed dot lines stand for the atmospheric p_{CO_2} of 40 Pa, at the exhaust gases p_{CO_2} of $15 \cdot 10^3$, and at the p_{CO_2} pure CO_2 stream generation of 10^5 Pa. Atomic top and sides views of CO_2 adsorbed on sites of MXene (0001) surfaces and TMC(111) surfaces, where top and inner layer M atoms are shown as dark and light blue spheres, respectively, whereas inner carbon layer is represented by dark yellow spheres. The CO_2 molecule oxygen and carbon atoms are represented by red and brown spheres, respectively. Adapted from data of Ref. 267.

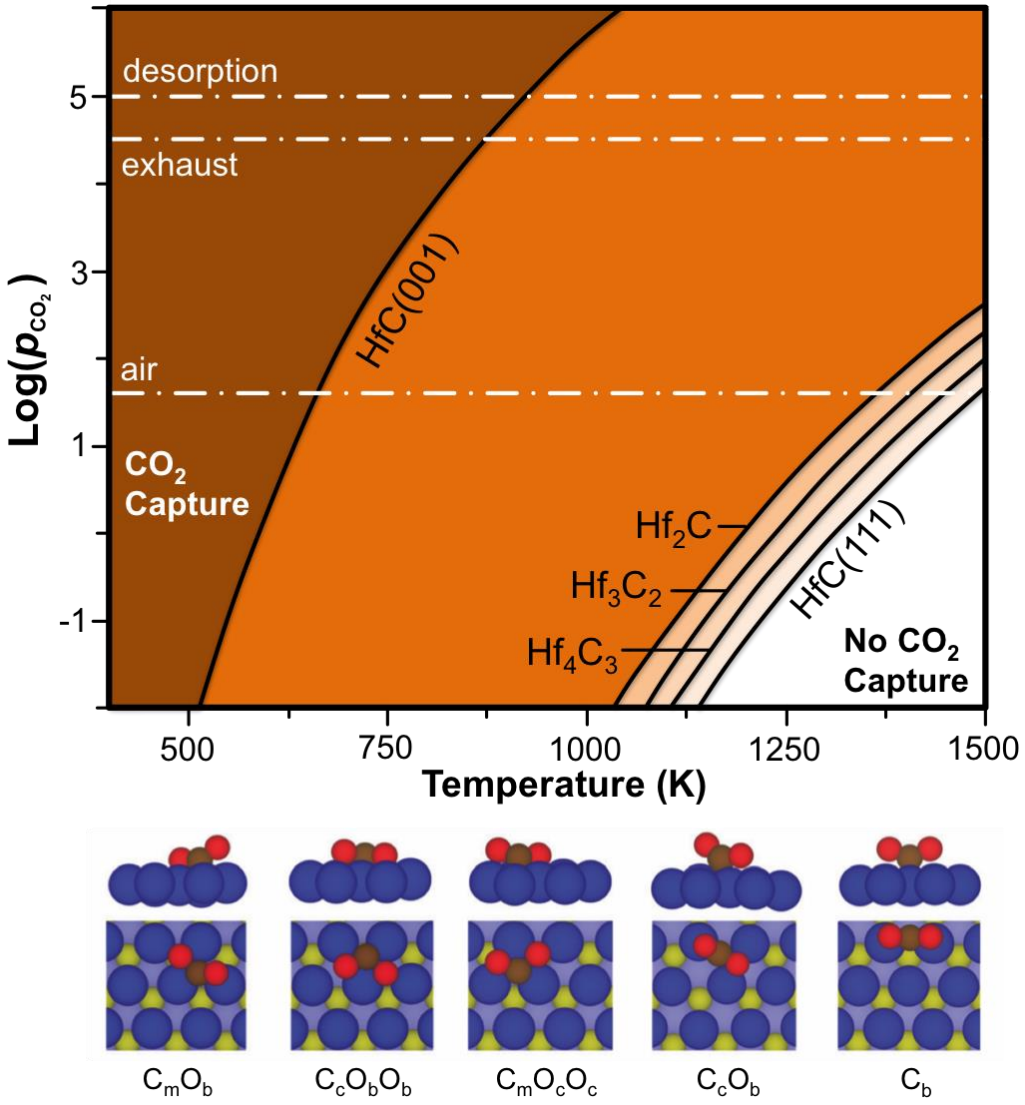

Figure 8 Gibbs free energy profile of the dry reforming of CH_4 catalysed by the (0001) surface of partially oxidized Mo_2C MXene at 1073 K, with CH_4 and CO_2 partial pressures of 1 bar. Insets show top views of critical reaction steps, where pink, red, black, and white spheres denote Mo, O, C, and H atoms, respectively.

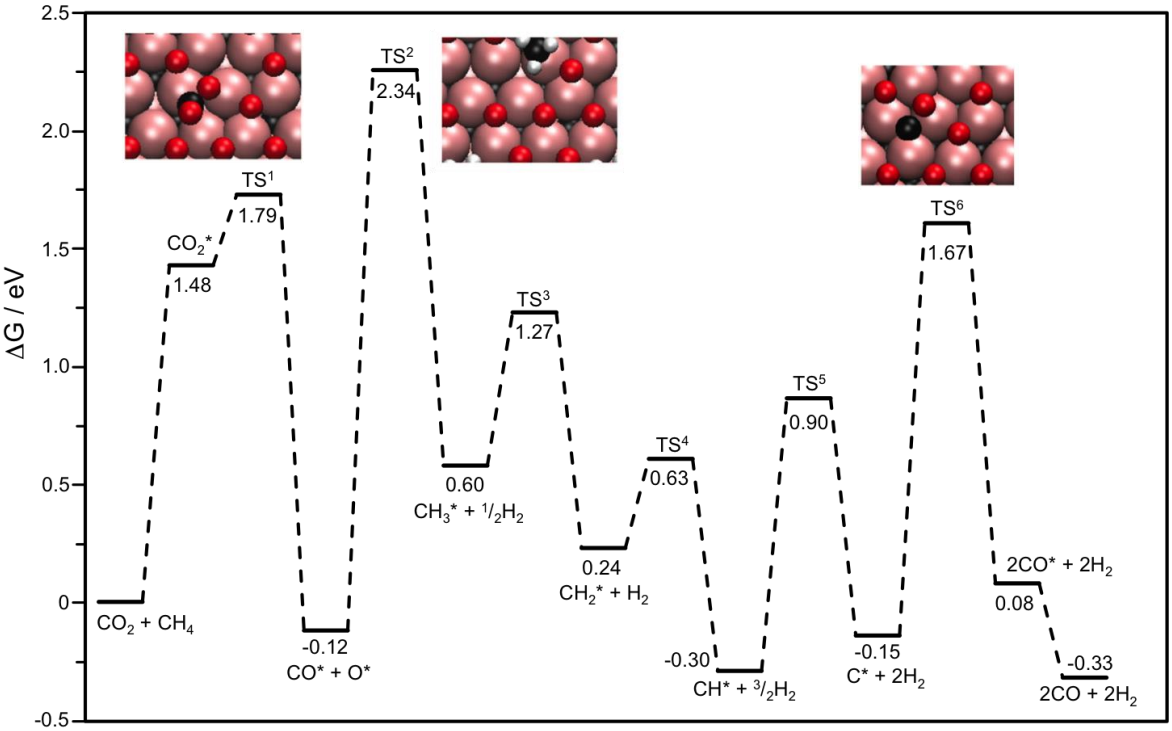

References

1. Thomas JM, Thomas WJ. Principles and practice of heterogeneous catalysis. Wiley-VCH: Weinheim, 2015.

2. Deutschmann O, Knözinger H, Kochloefl K, Turek T. Heterogeneous Catalysis and Solid Catalysts, 2. Development and Types of Solid Catalysts, in Ullmann's Encyclopedia of Industrial Chemistry; Wiley-VCH: Weinheim, 2011.

3. Liu L, Corma A. Metal Catalysts for Heterogeneous Catalysis: From Single Atoms to Nanoclusters and Nanoparticles. *Chem Rev.* 2018;*118*:4981–5079.

4 Somorjai GA, Limin Y. Introduction to Surface Chemistry and Catalysis, Wiley, 2010. ISBN: 978-0-470-50823-

5 Nørskov JK, Studt F, Abild-Pedersen F, Bligaard, T. Fundamental Concepts in Heterogeneous Catalysis. Wiley 2014, ISBN: 9781118888957. 4

6. Understanding Global Warming Potentials, United States Environmental Protection Agency, Available at: https://www.epa.gov/ghgemissions/understanding-global-warming-potentials, Accessed 14 January 2021.

7. Sources of Greenhouse Gas Emissions, United States Environmental Protection Agency, Available at: https://www.epa.gov/ghgemissions/sources-greenhouse-gas-emissions, Accessed 14 January 2021.

8. Sources of Climate Change: Atmospheric Carbon Dioxide, Available at: https://www.climate.gov/news-features/understanding-climate/climate-change-atmospheric-carbon-dioxide, Accessed 6 March 2021.

9. Sources of Our World in Data CO_2 Emissions, Available at: https://www.ourworldindata.org/co2-emissions, Accessed 6 March 2021.

10. COP 21 Paris France Sustainable Innovation Forum 2015, Climate Action & UNEP, Available at: http://www.cop21paris.org/, Accessed 14 January 2021.

11. Chen BWJ, Xu L, Mavrikakis M. Computational Methods in Heterogeneous Catalysis. *Chem Rev* 2021;*121*:1007−1048.

12. Pérez-Sánchez G, Chien SC, Gomes JRB, Cordeiro MNDS, Auerbach SM, Monson PA, Jorge M. Multiscale Model for the Templated Synthesis of Mesoporous Silica: The Essential Role of Silica Oligomers. *Chem Mater.* 2016;*28*:2715-2727.

13. Viñes F, Lamiel-García O, Illas F, Bromley ST. Size dependent structural and polymorphic transitions in ZnO: from nanocluster to bulk. *Nanoscale*. 2017;*9*:10067-10074.

14. Blum V, Gehrke R, Hanke F, Havu P, Havu V, Ren X, Reuter K, Scheffler M. Ab initio molecular simulations with numeric atom-centered orbitals. *Comp Phys Commun*. 2009;*180*:2175-2196.

15. Ramabhadran RO, Raghavachari K. Extrapolation to the gold-standard in quantum chemistry: computationally efficient and accurate CCSD(T) energies for large

molecules using an automated thermochemical hierarchy. *J Chem Theory Comput*. 2013;*9*:3986-3994.

16. Frisch MJ, Trucks GW, Schlegel HB, Scuseria GE, Robb MA, Cheeseman JR, Scalmani G, Barone V, Petersson GA, Nakatsuji H, Li X, Caricato M, Marenich A, Bloino J, Janesko BG, Gomperts R, Mennucci B, Hratchian HP, Ortiz JV, Izmaylov AF, Sonnenberg JL, Williams-Young D, Ding F, Lipparini F, Egidi F, Goings J, Peng B, Petrone A, Henderson T, Ranasinghe D, Zakrzewski VG, Gao J, Rega N, Zheng G, Liang W, Hada M, Ehara M, Toyota K, Fukuda R, Hasegawa J, Ishida M, Nakajima T, Honda Y, Kitao O, Nakai H, Vreven T, Throssell K, Montgomery Jr. JA, Peralta JE, Ogliaro F, Bearpark M, Heyd JJ, Brothers E, Kudin KN, Staroverov VN, Keith T, Kobayashi R, Normand J, Raghavachari K, Rendell A, Burant JC, Iyengar SS, Tomasi J, Cossi M, Millam JM, Klene M, Adamo C, Cammi R, Ochterski JW, Martin RL, Morokuma K, Farkas O, Foresman JB, Fox DJ. Gaussian 09, Revision A.02, Gaussian, Inc., Wallingford CT, 2016.

17. Furche F, Ahlrichs R, Hättig C, Klopper W, Sierka M, Weigend F. Turbomole. *WIREs Comput Mol Sci*. 2014;*4*:91-100.

18. Aprà E, Bylaska EJ, de Jong WA, Govind N, Kowalski K, Straatsma TP, Valiev M, van Dam HJJ, Alexeev Y, Anchell J, Anisimov V, Aquino FW, Atta-Fynn R, Autschbach J, Bauman NP, Becca JC, Bernholdt DE, Bhaskaran-Nair K, Bogatko S, Borowski P, Boschen J, Brabec J, Bruner A, Cauët E, Chen Y, Chuev GN, Cramer CJ, Daily J, Deegan MJO, Dunning Jr. TH, Dupuis M, Dyall KG, Fann GI , Fischer SA, Fonari A, Früchtl H, Gagliardi L, Garza J, Gawande N, Ghosh S, Glaesemann K, Götz AW, Hammond J, Helms V, Hermes ED, Hirao K, Hirata S, Jacquelin M, Jensen L, Johnson BG, Jónsson H, Kendall RA, Klemm M, Kobayashi R, Konkov V, Krishnamoorthy S, Krishnan M, Lin Z, Lins RD, Littlefield RJ, Logsdail AJ, Lopata K, Ma W, Marenich AV, Martin del Campo J, Mejia-Rodriguez D, Moore JE, Mullin JM, Nakajima T, Nascimento DR, Nichols JA, Nichols PJ, Nieplocha J, Otero-de-la-Roza A, Palmer B, Panyala A, Pirojsirikul T, Peng B, Peverati R, Pittner J, Pollack L, Richard RM, Sadayappan P, Schatz GC, Shelton WA, Silverstein DW, Smith DMA, Soares TA, Song D, Swart M, Taylor HL, Thomas GS, Tipparaju V, Truhlar DG, Tsemekhman K, Van Voorhis T, Vázquez-Mayagoitia Á, Verma P, Villa O, Vishnu A, Vogiatzis KD, Wang D, Weare JH, Williamson MJ, Windus TL, Woliński K, Wong AT, Wu Q, Yang C, Yu Q, Zacharias M, Zhang Z, Zhao Y, Harrison RJ. NWChem: Past, present, and future. *J Chem Phys.* 2020;152:184102.

19. Neese F. Software update: the ORCA program system, version 4.0. *Wiley Interdiscip Rev Comput Mol Sci.* 2017;*8*:e1327.

20. Schmidt W, Baldridge KK, Boatz JA, Elbert ST, Gordon MS, Jensen JH, Koseki S, Matsunaga N, Nguyen KA, Su S, Windus TL, Dupuis M, Montgomery JA. General Atomic and Molecular Electronic Structure System. *J Comput Chem.* 1993;*14*: 1347-1363.

21. Mele F, Russo N, Illas F. Theoretical Study of the interaction of alkali-metal atoms with CO_2. *Chem Phys Lett*. 1998;*295*:409-415.

22. Knurr BJ, Weber JM. Solvent-driven reductive activation of carbon eioxide by Gold anions. *J Am Chem Soc*. 2012;*134*:18804-18808.

23. Thompson MC, Ramsay J, Weber JM. Solvent-driven reductive activation of CO_2 by Bismuth: switching from metalloformate complexes to oxalate products. *Angew Chem Int Ed*. 2016;*55*:15171-15174.

24. Koyanagi GK, Bohme DK. Gas-phase reactions of carbon dioxide with atomic transition-metal and main-group cations: room-temperature kinetics and periodicities in reactivity. *J Phys Chem A*. 2006;*110*:1232-1241.

25. Zhao Z, Kong X, Yuan Q, Xie H, Yang D, Zhao J, Fan H, Jiang L. Coordination-induced CO_2 fixation into carbonate by metal oxides. *Phys Chem Chem Phys*. 2018;*20*:19314-19320.

26. de Heer WA. The physics of simple metal clusters: experimental aspects and simple models. *Rev Mod Phys*. 1993;*65*:611-673.

27. Haertelt M, Fielicke A, Meijer G, Kwapien K, Sierka M, Sauer J. Structure determination of neutral MgO clusters-hexagonal nanotubes and cages. *Phys Chem Chem Phys*. 2012;*14*:2849-2856.

28. Jimenez-Izal E, Aleksandrova AN. Computational design of clusters for catalysis. *Annu Rev Phys Chem*. 2018;*69*:377–400.

29 Abbet S, Judai K, Klinger L, Heiz U. Synthesis of monodispersed model catalysts using softlanding cluster deposition. *Pure Appl Chem.* 2020,74:1527-1535.

30. Lee SS, Fan CY, Wu TP, Anderson SL. CO oxidation on Au_n/TiO_2 catalysts produced by size-selected cluster deposition. *J Am Chem Soc*. 2004;*126*:5682–5683.

31. Viñes F, Carrasco J, Bromley ST. Nanoscale thermal stabilization via permutational premelting. *Phys Rev B.* 2012;*85*: 195425.

32. Gomes JRB, Gomes JANF. A DFT study of the methanol oxidation catalyzed by a copper surface. *Surf Sci.* 2001;*471*:59-70.

33. Klüner T, Govid N, Wang YA, Carter EA. Prediction of electronic excited states of adsorbates on metal surfaces from first principles. *Phys Rev Lett*. 2001;*26*:5954.

34 Pacchioni G, Ferrari AM, Marquez AM, Illas F. Importance of Madelung potential in quantum chemical modeling of ionic surfaces. *J Comput Chem*. 1996;18:617-628.

35 Sousa C, Tosoni S, Illas F. Theoretical approaches to excited states related phenomena in oxide surfaces. *Chem Rev.* 2013;113:4456-4495

36. Gomes JRB, Illas F, Cruz-Hernández N, Márquez A, Sanz JF. Interaction of Pd with α-Al_2O_3(0001): A case study of modeling the metal-oxide interface on complex substrates. *Phys Rev B.* 2002;65:125414.

37. Guo Y, Langlois JM, Goddard III WA. Electronic structure and valence-bond band structure of cuprate superconducting materials. *Science*. 1998;*239*:896-899.

38. Gomes JRB, Illas F, Silvi B. Topological analysis of the metal-support interaction: the case of Pd atoms on oxide surfaces. *Chem Phys Lett*. 2004;388:132-138.

39. Sauer J. Molecular models in ab initio studies of solids and surfaces: from ionic crystals and semiconductors to catalysts. *Chem Rev*. 1989;*89*:1-199.

40. Bloch F. Über die Quantenmechanik der Elektronen in Kristallgittern. *Z. Phys*. 1928;*52*:555-600.

41. Kresse G, Furthmüller J. Efficient iterative schemes for *ab initio* total-energy calculations using a plane-wave basis set. *Phys Rev B*. 1996;*54*:11169-11186.

42. Dovesi R, Erba A, Orlando R, Zicovich-Wilson CM, Civalleri B, Maschio L, Rerat M, Casassa S, Baima J, Salustro S, Kirtman B. Quantum-mechanical condensed matter simulations with CRYSTAL. *WIREs Comput Mol Sci*. 2018;*8*:e1360.

43. Başaran K, Topçubaşı BU, Davran-Candan T. Theoretical investigation of CO_2 adsorption mechanism over amine-functionalized mesoporous silica. *J. CO_2 Util.* 2021;*47*:101492.

44. Afonso R, Sardo M, Mafra L, Gomes JRB. Unravelling the Structure of Chemisorbed CO_2 Species in Mesoporous Aminosilicas: A Critical Survey. *Environ. Sci. Technol.* 2019;*53*:2758–2767.

45. Bao JL, Carter EA. Surface-Plasmon-induced ammonia decomposition on copper: excited-state reaction pathways revealed by embedded correlated wavefunction theory. *ACS Nano*. 2019;*13*:9944−9957.

46. Zhao Q, Zhang X, Martirez JMP, Carter EA. Benchmarking an embedded adaptive sampling configuration interaction method for surface reactions: H_2 desorption from and CH_4 dissociation on Cu(111). *J. Chem. Theory Comput.* 2020;*16*:7078-7088.

47. Bagus PS, Illas F, *Encyclopedia of Computational Chemistry*, Schleyer PvR, Allinger NL, Clark T, Gasteiger J, Kollman PA, Schaefer III HF, Schreiner PR, Eds.; John Wiley & Sons: Chichester, UK, 1998;*4*:2870-2887.

48. Baletto F, Ferrando, R. Structural properties of nanoclusters: Energetic, thermodynamic, and kinetic effects. *Rev Mod Phys*. 2005;*77*:371-423.

49. Ferrando R, Jellinek J, Johnston, RL. Nanoalloys: from theory to applications of alloy clusters and nanoparticles. *Chem Rev*. 2008;*108*:845-910.

50. Catlow CRA, Bromley ST, Hamad S, Mora-Fonz M, Sokola AA, Woodley SM. Modelling nano-clusters and nucleation. *Phys Chem Chem Phys*. 2010;*12*:786-811.

51. Wulff G. Zur Frage der Geschwindigkeit des Wachsturms under Auflösung der Kristallflächen. *Z Kristallogr*. 1901;*34*:449-530.

52. Desjonqueres MC, Spanjaard D. *Concepts in Surface Physics*, Springer-Verlag, Berlin 1996.

53. Viñes F, Gomes JRB, Illas, F. Understanding the reactivity of metallic nanoparticles: beyond the extended surface model for catalysis. *Chem Soc Rev*. 2014;*43*:4922-4939.

54. Barnard AS, Zapol P. A model for the phase stability of arbitrary nanoparticles as a function of size and shape. *J Chem Phys*. 2004;*121*:4276-4283.

55 González D, Camino B, Heras-Domingo J, Rimola A, Rodríguez-Santiago L, Solans-Monfort X, Sodupe M. A Free Computational Tool for Generating Wulff-like Nanoparticle Models with Controlled Stoichiometry, *J Phys Chem C*. 2020; 124: 1227-1237.

56. Bromley ST, Moreira IdPR, Neyman KM, Illas F. Approaching nanoscale oxides: models and theoretical methods. *Chem Soc Rev*. 2009;*28*:2657-2670.

57. Yudanov IV, Sahnoun R, Neyman KM, Rösch N. Scalable properties of metal clusters: A comparative study of modern exchange-correlation functionals. *J Chem Phys*. 2002;*117*:9887–9896.

58. Yudanov IV, Neyman KM, Rösch N. C–O bond scission of methoxide on Pd nanoparticles: a density functional study. *Phys Chem Chem Phys*. 2006;*8*:2396–2401.

59. Lamiel-García O, Ko KC, Lee JY, Bromley ST, Illas F. When anatase nanoparticles become bulklike: properties of realistic TiO_2 nanoparticles in the 1–6 nm size range from all electron relativistic density functional theory based calculations. *J Chem Theory Comput*. 2017;*13*:1785-1793.

60. Morales-García Á, Valero R, Illas F. Reliable and computationally affordable prediction of the energy gap of $(TiO_2)_n$ ($10 \leq n \leq 563$) nanoparticles from density functional theory. *Phys Chem Chem Phys.* 2018;*20*:18907-18911.

61. Morales-García Á, Macià, A, Illas, F, Bromley ST. Understanding the interplay between size, morphology and enery gap in photoactive TiO_2 nanoparticles. *Nanoscale* 2019;*11*:9032-9041.

62. Yudanov IV, Matveev AV, Neyman KM, Rösch N. How the C−O bond breaks during methanol decomposition on nanocrystallites of palladium catalysts. *J Am Chem Soc*. 2008;*130*:9342-9352.

63. Chang CR, Wang YG, Li J. Theoretical investigations of the catalytic role of water in propene epoxidation on gold nanoclusters: a hydroperoxyl-mediated pathway. *Nano Res*. 2011; *4*:131-142.

64. Filot IAW, Shetty SG, Hensen EJM, van Santen RA. Size and topological effects of Rhodium surfaces, clusters and nanoparticles on the dissociation of CO. *J Phys Chem C*. 2011;*115*:14204-14212.

65. Eichler A, Hafner J. Molecular precursors in the dissociative adsorption of O_2 on Pt(111). *Phys Rev Lett*. 1997;*79*:4481-4484.

66. Bates SP, Kresse G, Gillan MJ. The adsorption and dissociation of ROH molecules on TiO_2(110). *Surf Sci*. 1998;*409*:336-349.

67. Dong W, Hafner J. H_2 dissociative adsorption on Pd(111). *Phys Rev B*. 1997;*56*: 15396-15403.

68. Gomes JRB, Fajín JLC, Cordeiro MNDS, Teixeira C, Gomes P, Pillai RS, Novell-Leruth G, Toda J, Jorge M. Density functional treatment of interactions and chemical reactions at interfaces (Chapter 1), in (Eds) Morin J, Pelletier JM. Density

Functional Theory: Principles, Applications and Analysis, Nova Science Publishers, New York, 2013.

69. Sholl DS, Steckel JA. Density Functional Theory: A Practical Introduction (Chapter 4), John Wiley & Sons, Inc., New Jersey, 2009.

70. Sun W, Ceder G. Efficient creation and convergence of surface slabs. Surf Sci 2013; *617*:53-59.

71. Jiang X, Nie X, Gong Y, Moran CM, Wang J, Zhu J, Chang H, Guo X, Walton KS, Song C. A combined experimental and DFT study of H_2O effect on In_2O_3/ZrO_2 catalyst for CO_2 hydrogenation to methanol. *J Catal*. 2020;*383*:283-296.

72. Monte M, Gamarra D, López Cámara A, Rasmussen SB, Gyorffy N, Schay Z, Martínez-Arias A, Conesa JC. Preferential oxidation of CO in excess H_2 over CuO/CeO_2 catalysts: Performance as a function of the copper coverage and exposed face present in the CeO_2 support. *Catal Today*. 2014;*229*:104-113.

73. Jimenez-Orozco C, Flórez E, Viñes F, Rodriguez JA, Illas F. Critical hydrogen coverage effect on the hydrogenation of ethylene catalyzed by δ-MoC(001): an *ab initio* thermodynamic and kinetic study. *ACS Catal*. 2020;*10*:6213-6222.

74. Pajares A, Prats H, Romero A, Viñes F, Ramírez de la Piscina P, Sayós R, Homs N, Illas F. Critical effect of carbon vacancies on the reverse water gas shift reaction over vanadium carbide catalysts. *Appl Catal B: Environ*. 2020;*267*:118719.

75. Logsdail AJ, Downing CA, Keal TW, Sherwood P, Sokol AA, Catlow CRA. Hybrid-DFT modeling of lattice and surface vacancies in MnO. *J Phys Chem C*. 2019;*123*: 8133-8144.

76. Tian D, Li K, Wei Y, Zhu X, Zeng C, Cheng X, Zhenga Y, Wang H. DFT insights into oxygen vacancy formation and CH_4 activation over CeO_2 surfaces modified by transition metals (Fe, Co and Ni). *Phys Chem Chem Phys*. 2018;*20*:11912-11929.

77. Favaro M, Xiao H, Cheng T, Goddard III WA, Yano J, Crumlin EJ. Subsurface oxide plays a critical role in CO_2 activation by Cu(111) surfaces to form chemisorbed CO_2, the first step in reduction of CO_2. *Proc Natl Acad Sci*. 2017;*114*:6706-6711.

78. Sun Y, Cao Y, Wang L, Mu X, Zhao Q, Si R, Zhu X, Chen S, Zhang B, Chen D, Wan Y. Gold catalysts containing interstitial carbon atoms boost hydrogenation activity. *Nat Commun*. 2020;*11*:4600.

79. Piqué O, Koleva IZ, Viñes F, Aleksandrov HA, Vayssilov GN, Illas F. Subsurface carbon: a general feature of noble metals. *Angew Chem Int Ed*. 2019;*58*:1744-1748.

80. Yang W, Gao Z, Liu X, Ma C, Ding X, Yan W. Directly catalytic reduction of NO without NH_3 by single atom iron catalyst: A DFT calculation. *Fuel* 2019;*243*:262-270.

81. Koleva IZ, Aleksandrov HA, Neyman KM, Vayssilov GN. Preferential location of zirconium dopants in cerium dioxide nanoparticles and the effects of doping on their reducibility: a DFT study. *Phys Chem Chem Phys*. 2020;*22*:26568-26582.

82. Righi G, Magri R, Selloni A. H_2 dissociation on noble metal single atom catalysts adsorbed on and doped into CeO_2(111). *J Phys Chem C*. 2019;*123*:9875-9883.

83. Li X, Wang S, Zhu Y, Yang G, Zheng P. DFT study of bio-oil decomposition mechanism on a Co stepped surface: Acetic acid as a model compound. *Int J Hydrog Energy*. 2015;*40*:330-339.

84. Hussain A, Curulla Ferré D, Gracia J, Nieuwenhuys BE, Niemantsverdriet W. DFT study of CO and NO adsorption on low index and stepped surfaces of gold. *Surf Sci*. 2009;*603*:2734-2741.

85. Orita H, Inada Y. DFT investigation of CO adsorption on Pt(211) and Pt(311) surfaces from low to high coverage. *J Phys Chem B*. 2005;*109*:69-75.

86. Fajín JLC, Gomes JRB, Cordeiro MNDS. DFT study of the adsorption of D-(L-)cysteine on flat and chiral stepped gold surfaces. *Langmuir* 2013;*29*:8856-8864.

87. Šljivančanin Ž, Gothelf KV, Hammer B. Density functional theory study of enantiospecific adsorption at chiral surfaces. *J Am Chem Soc*. 2002;*124*:14789-14794.

88. Viñes F, Lamiel-García O. Approaching the quantitative description of enantioselective adsorption by the density functional theory means. *J Phys Chem C*. 2019;*123*:11714-11722.

89. Liu X, Kunkel C, Ramírez de la Piscina P, Homs N, Viñes F, Illas F. Effective and highly selective CO Generation from CO_2 using a polycrystalline α-Mo_2C catalyst. *ACS Catal*. 2017;*7*:4323-4335.

90. Ungerer MJ, Santos-Carballal D, Cadi-Essadek A, van Sittert CGCE, de Leeuw NH. Interaction of SO_2 with the Platinum (001), (011), and (111) surfaces: a DFT study. *Catalysts* 2020;*10*:558.

91. Silveri F, Quesne MG, Roldán A, de Leeuw NH, Catlow CRA. Hydrogen adsorption on transition metal carbides: a DFT study. *Phys Chem Chem Phys*. 2019;*21*:5335-5343.

92. Viñes F, Lykhach Y, Staudt T, Lorenz MPA, Papp C, Steinrück H-P, Libuda J, Neyman KM, Görling A. Methane activation by Platinum: critical role of edge and corner sites of metal nanoparticles. *Chem Eur J*. 2010;*16*:6530-6539.

93. Fajín JLC, Bruix A, Cordeiro MNDS, Gomes JRB, Illas F. Density functional theory model study of size and structure effects on water dissociation by platinum nanoparticles. *J Chem Phys.* 2012;*137*:034701.

94. Kozlov SM, Neyman KM. Insights from methane decomposition on nanostructured Palladium. *J Catal*. 2016;*337*:111-121.

95. Al Abdulghani AJ, Park J-H, Kozlov SM, Kang D-C, AlSabban B, Pedireddy S, Aguilar-Tapia A, Ould-Chikh S, Hazemann J-L, Basset J-M, Cavallo L, Takanabe K. Methane dry reforming on supported cobalt nanoparticles promoted by boron. *J Catal*. 2020;*392*:126-134.

96. Kozlov SM, Aleksandrov HA, Neyman KM. Energetic stability of absorbed H in Pd and Pt nanoparticles in a more realistic environment. *J Phys Chem C*. 2015;*119*:5180-5186.

97. Suchorski Y; Kozlov SM, Bespalov I, Datler M, Vogel D, Budinska Z, Neyman KM, Rupprechter G. The role of metal/oxide interfaces for long-range metal particle activation during CO oxidation. *Nat Mater*. 2018;*17*:519–522.

98. Qureshi M, Garcia-Esparza AT, Jeantelot G, Ould-Chikh S, Aguilar-Tapia A, Hazemann J-L, Basset J-M, Loffreda D, Le Bahers T, Takanabe K. Catalytic consequences of ultrafine Pt clusters supported on $SrTiO_3$ for photocatalytic overall water splitting. *J Catal*. 2019;*376*:180-190.

99. Li, Z, Ji S, Liu Y, Cao X, Tian S, Chen Y, Niu Z, Li Y. Well-defined materials for heterogeneous catalysis: from nanoparticles to isolated single-atom sites. *Chem Rev*. 2020;*120*:623-682.

100. Pei W, Zhou S, Zhao J, Xu X, Du Y, Dou SY. Immobilized trimeric metal clusters: a family of the smallest catalysts for selective CO_2 reduction toward multi-carbon products. *Nano Energy.* 2020;*76*:105049.

101. Li M, Borsay A, Dakhchoune M, Zhao K, Luo W, Züttel A. Thermal stability of size-selected copper nanoparticles: effect of size, support and CO_2 hydrogenation atmosphere. *Appl Surf Sci.* 2020;*510*:145439.

102. Liu L, Lv P. Understanding the enhanced catalytic activity of bimetallic $AuCu/TiO_2$ in CO_2 adsorption and activation: a density functional theory study. *New J Chem*. 2020;*44*:14662.

103. Zhai H, Sautet P, Alexandrova AN. Global optimization of adsorbate covered supported cluster catalysts: the case of $Pt_7H_{10}CH_3$ on alpha-Al_2O_3. *ChemCatChem*. 2020;*12*:762-770.

104. Prats H, Gutiérrez RA, Piñero JJ, Viñes F, Bromley ST, Ramírez PJ, Rodriguez JA, Illas F. Room temperature methane capture and activation by Ni clusters supported on TiC(001): effects of metal-carbide interactions on the cleavage of the C-H bond. *J Am Chem Soc*. 2019;*141*:5303-5313.

105. Kaiser SK, Chen Z, Akl DF, Mitchell S, Pérez-Ramírez. Single-Atom Catalysts across the Periodic Table. *Chem Rev.* 2020;*120*:11703-11809.

106. Vanbuel J, Ferrari P, Janssen. Few-atom cluster model systems for a hydrogen economy. *Adv Phys-X.* 2020;*5*:1754132.

107. Margraf JT, Reuter K. Systematic enumeration of elementary reaction steps in surface catalysis. *ACS Omega.* 2019;*4*:3370-3379.

108. Bruix A, Margraf JT, Andersen M, Reuter K. First-principles-based multiscale modelling of heterogeneous catalysis. *Nat Catal.* 2019;*2*:659-670.

109. Nørskov JK, Bligaard T, Rossmeisl J, Christensen CH. Towards the computational design of solid catalysts. *Nat Chem.* 2009;*1*:37.

110. Nørskov JK, Abild-Pedersen F, Studt F, Bligaard T. Density functional theory in surface chemistry and catalysis. *Proc Natl Acad Sci.* 2011;*108*:937-943.

111. Hohenberg P, Kohn W. Inhomogeneous electron gas. *Phys Rev B.* 1964;*136*: 864-871.

112. Kulkari, A, Siahrostami, S, Pater, A, Nørskov JK. Understanding catalytic activity trends in the oxygen reduction reaction. *Chem Rev.* 2018;*118*:2302-2312.

113. Zhu CR, Gao D, Ding J, Chao D, Wang J. TMD-based highly efficient electrocatalysts developed by combined computational and experimental approaches. *Chem Soc Rev.* 2018;*47*:4332-4356.

114. Krylov A, Windus TL, Barnes T, Marín-Rimoldi E, Nash JA, Pritchard B, Smith DGA, Altarawy D, Saxe P, Clementi C, Crawford TD, Harrison RJ, Jha S, Pande VS, Head-Gordon T. Perspective: Computational chemistry software and its advancement as illustrated through three grand challenge cases for molecular science. *J Chem Phys.* 2018;*149*:180901.

115. Karton A. A computational chemist´s guide to accurate thermochemistry for organis molecules. *WIREs Comput Mol Sci.* 2016;*6*:292-310.

116. Novikov AS. Computational insights into industrial chemistry. *Computation* 2020;*8*:97.

117. Drummond B. Understanding quantum mechanics: a review and synthesis in precise language. *Open Phys.* 2019;*17*:390-437.

118. Jensen F. Introduction to Computational Chemistry, 3rd Edition, 2017. Wiley, ISBN: 978-1-118-82599-0.

119. Hohenberg P, Kohn W. Inhomogeneous Electron Gas. *Phys Rev.* 1964;*136*:B864-B871.

120. Kohn W, Sham LJ. Self-consistent equations including exchange and correlation effects. *Phys Rev.* 1965;*140*:A1133-A1138.

121. Woods ND, Payne MC, Hasnip PJ. Computing the self-consistent field in Kohn-Sham density functional theory. *J Phys Condens Matter.* 2019;*31*:453001.

122. Boese AD, Martin JML, Handy NC. The role of the basis set: Assessing density functional theory. *J Chem Phys.* 2003;*119*:3005-3014.

123. Mardirossian N, Head-Gordon M. Thirty years of density functional theory in computational chemistry: an overview and extensive assessment of 200 density functionals. *Mol Phys.* 2017;*115*:2315-2372.

124. Vega L, Viñes F. Generalized gradient approximation adjusted to transition metals properties: Key roles of exchange and local spin density. *J Comput Chem*. 2020;*41*:2598-2603.

125. Wiitala KW, Hope TR, Cramer CJ. Hybrid density functional methods empirically optimized for the computation of ^{13}C and ^{1}H chemical shifts in chloroform solution. *J Chem Theory Comput*. 2006;*2*:1085-1092.

126. Jin Y, Barlett RJ. Accurate Computation of X-ray absorption spectra with ionization potential optimized global hybrid functional. *J Chem Phys.* 2018;*149*: 064111.

127. Sarmiento.Pérez R, Botti, S, Marques MAL. Optimized Exchange and correlation semilocal functional for the calculation of energies of formation. *J Chem Theory Comput*. 2015;*11*:3844-3850.

128. Tran F, Blaha P. Accurate band gaps of semiconductors and insulators with a semilocal exchange-correlation potential. *Phys Rev Lett.* 2009;*102*:226401.

129. Perdew JP, Schmidt K. Jacob´s ladder of density functional approximations for the exchange-correlation energy. *AIP Conf Proc.* 2001;*577*:1-20.

130. Jones RO. Energy surface of low-lying states of O_3 and SO_2. *J Chem Phys.* 1985;*82*:325-332.

131. Lang ND, Nørskov JK. Interaction of helium with a metal-surface. *Phys Rev B.* 1983;*27*:4612-4616.

132. Perdew JP, Wang Y. Accuarte and simple analytic representation of the electron-gas correlation-energy. *Phys Rev B.* 1992;*45*:13244-13249.

133. Perdew JP, Burke K, Ernzerhof M. Generalized gradient approximation made simple. *Phys Rev Lett.* 1996;*77*:3865-3868.

134. Hammer B, Hansen LB, Nørskov JK. Improved adsorption energetics within density-functional theory using revised Perdew-Burke-Erzerhof functionals. *Phys Rev B.* 1999;*59*:7413-7421.

135. Perdew JP, Ruzsinzsky A, Csonka GI, Vydrov OA, Scuseria GE, Constantin LA, Zhou X, Burke K. Restoring the density-gradient expansion for exchange in solids and surfaces. *Phys Rev Lett.* 2008;*100*:136406.

136. Becke AD. Density-functional exchange-energy approximation with correct asymptotic-behavior. *Phys. Rev. A.* 1988;*38*:3098-3100.

137. Hammer B, Scheffler M, Jacobsen KW, et al. Multidimensional potential-energy surface for H_2 dissociation over Cu(111). *Phys Rev Lett.* 1994;*73*:1400-1403.

138. Becke AD. A new inhomogeneity parameter in density-functional theory. *J Chem Phys.* 1998;*109*:2092-2098.

139. Medasani B, Haranczyk M, Canning A. et al. Vacancy formation energies in metals: a comparison of MetaGGA with LDA and GGA exchange-correlation functionals. *Comput Mater Sci.* 2015;*101*:96-107.

140. Becke AD. Density functional thermochemistry. III. The role of exact exchange. *J Chem Phys*. 1993;*98*:5648-5652.

141. Cramer CJ, Truhlar DG. Density functional theory for transition metals and transition metal chemistry. *Phys Chem Chem Phys.* 2009;*11*:10757–10816.

142. Vega L, Ruvireta J, Viñes F, Illas F. Jacob's Ladder as Sketched by Escher: Assessing the Performance of Broadly Used Density Functionals on Transition Metal Surface Properties. *J Chem Theory Comput.* 2018;*14*:395-403.

143. Prates Ramalho JP, Gomes JRB, Illas F. Accounting for van der Waals interactions between adsorbates and surfaces in density functional theory based calculations: selected examples. *RSC Adv*. 2013;*3*:13085-13100.

144. Klimeš J, Michaelides A. Perspective: advances and challenges in treating van der Waals dispersion forces in density functional theory. *J Chem Phys.* 2012;*137*:120901-120912.

145. Grimme S. Accurate description of van der Waals complexes by density functional theory including empirical corrections. *J Comput Chem* 2004;*25*:1463-1473.

146. Grimme S, Antony J, Ehrlich S, Krieg H. A consistent and accurate ab initio parametrization of density functional dispersion correction (DFT-D) for the 94 elements H-Pu. *J Chem Phys* 2010;*132*:154104-154119.

147. Tkatchenko A, Scheffler M. Accurate molecular van der Waals interactions from ground-state electron density and free-atom reference data. *Phys Rev Lett* 2009;*102*:073005-073008.

148. Klimes J, Bowler DR, Michaelides A. Chemical accuracy for the van der Waals density functionals. *J Phys Condens Matter* 2010;*22*:022201-022205.

149. Wellendorff J. Lundgaard KT, Møgelhøj A, Petzold V, Landis DD, Nørskov JK, Bligaard T, Jacobsen KW. Density functionals for surface science: exchange-correlation model development with Bayesian error estimation. *Phys Rev B.* 2012;*85*: 235149-235171.

150. Cohen AJ, Mori-Sánchez P, Yang WT. Insights into current limitations of density functional theory. *Science.* 2008:*321*; 792-794.

151. Dudarev SL, Botton GA, Savrasov SY, Humphreys CJ, Sutton AP. *Phys Rev B* 1998; 57: 1505.

152 Loschen C, Carrasco J, Neyman KM, Illas F. First Principles LDA+U and GGA+U Study of Cerium Oxides: Dependence on the Effective U-Parameter. *Phys Rev B* 2007:75: 035115.

153. Arroyo-de Dompablo ME, Morales-García Á, Taravillo M. DFT+*U* calculations of crystal lattice, electronic structure, and phase stability under pressure of TiO_2 polymorphs. *J Chem Phys.* 2011:*135*;054503.

154 Payne MC, Teter MP, Allan DC, Arias TA, Joannopoulos JD. Iterative minimization techniques for ab initio total-energy calculations: molecular dynamics and conjugate gradients. *Rev Mod Phys.* 1992; 64: 1045−1097.

155 Wang LP, Song C. Car−Parrinello Monitor for More Robust Born−Oppenheimer Molecular Dynamics. *J Chem Theory Comput*. 2019; 15: 4454-4467.

156. Reuter K, Scheffler M. Composition, structure and stability of RuO_2(110) as a function of oxygen pressure. *Phys Rev B.* 2001:*65*;35406.

157. Reuter K, Scheffler M. Composition and structure of the RuO_2(110) surface in an O_2 and CO environment: implications for the catalytic formation of CO_2. *Phys Rev* B. 2003:68;45407.

158 Reuter K, Stampf C, Scheffler M. AB Initio Atomistic Thermodynamics and Statistical Mechanics of Surface Properties and Functions in Yip S. (eds). Handbook of Materials Modeling. 2005, 149-194. Springer, Dordrecht.

159. Henkelman G, Jóhannesson G, Jónsson H. *Methods for finding saddle points and minimum energy paths*. In: Schwartz SD, editor. *Theoretical methods in condensed phase chemistry*. New York (NY): Kluwer Academis; 2000. p. 269-300.

160. Henkelman G, Uberuaga BP, Jónsson H. A climbing image nudged elastic band method for finding saddle points and minimum energy paths. *J Chem Phys.* 2000:*113*;9901-9904.

161. Henkelman G, Jónsson H. A dimer method for finding saddle points on high dimensional potential surfaces using only first derivatives. *J Chem Phys.* 1999:*111*;7010-7022.

162. Fajín JLC, Cordeiro MNDS, Illas F, Gomes JRB. Influence of step sites in the molecular mechanism of the water gas shift reaction catalyzed by copper. *J Catal.* 2009;*268*:131-141.

163. Fajín JLC, Cordeiro MNDS, Illas F, Gomes JRB. Generalized Brønsted-Evans-Polanyi relationships and descriptors for O-H bond cleavage of organic molecules on transition metal surfaces. *J Catal.* 2014;*313*:24-33.

164 Heyden A, Bell AT, Keil FJ. Efficient Methods for Finding Transition States in Chemical Reactions: Comparison of Improved Dimer Method and Partitioned Rational Function Optimization Method. *J Chem Phys.* 2005;*123*:224101

165 Motagamwala AH, Dumesic JA. Microkinetic Modeling: A Tool for Rational Catalyst Design. *Chem Rev* 2021;*121*:1049−1076.

166. Stengelmann C, Andreasen A, Campbell CT. Degree of rate control: how much the energies of intermediates and transition states control rates. *J Am Chem Soc.* 2009:*131*;8077-8082.

167. Reaction Design, CHEMKIN 10131, 2013.

168. Goodwin DC, Speth RL, Moffat HK, Weber BW. Cantera: An object-oriented software toolkit for chemical kinetics, thermodynamics, and transport processes. Available at https://www.cantera.org, Accessed 10 October 2020).

169. Medford AJ, Shi C, Hoffmann MJ, Lausche AC, Fitzgibbon SR, Bligaard T, Nørskov JK. CatMAP: A software package for descriptor-based microkinetic mapping of catalytic trends. *Catal Lett.* 2015:*145*;794-807.

170. Filot IAW, van Santen RA, Hensen EJM. The optimally performing Fischer-Tropsch catalyst. *Angew Chem Int Ed.* 2014:*53*;12746-12750.

171. Hermes ED, Janes AN, Schmidt JR. Micki: A python-based object-oriented microkinetic modeling code. *J Chem Phys.* 2019:*151*;014112.

172. Stoltze P, Nørskov JK. An interpretation of the high-pressure kinetics of ammonia-synthesis based on a microscopic model. *J Catal.* 1988:*110*;1-10.

173 Gokhale AA, Dumesic JA, Mavrikakis M. On the Mechanism of Low-Temperature Water Gas Shift Reaction on Copper *J Am Chem Soc.* 2008;*130*:1402-1414.

174. Bhandari S, Rangarajan, S, Mavrikakis, M. Combining computational modeling with reaction kinetics experiments for elucidating the *in situ* nature of the active site in catalysis. *Acc Chem Res.* 2020:*53*;1893-1904.

175. Singh S, Li S, Carrasquillo-Flores R, Alba-Rubio AC, Dumesic JA, Mavrikakis M. Formic acid decomposition on Au catalysts: DFT, microkinetic modeling, and reaction kinetics experiments. *AIChE J.* 2014:*60*;1303-1319.

176. Helton JC, Johnson JD, Sallaberry CJ, Storlie CB. Survey of sampling-based methods for uncertainty and sensitivity analysis. *Reliab Eng Syst Saf.* 2006:*91*;1175-1209.

177. Frenkel D, Smit B. *Understanding molecular simulation: from algorithms to applications* (2nd Edition). Cambridge, MA: Academic Press. 2001.

178. Bortz AB, Kalos MH, Lebowitz JL. A new algorithm for Monte Carlo simulation of ising spin systems. *J Comput Phys.* 1975:*17*;10-18.

179. Jansen APJ, An introduction to kinetic Monte Carlo simulations of surface reactions, Lecture Notes in Physics, vol. 856, Springer-Verlag, Heidelberg, Germany, 2012.

180. Andersen M, Panosetti C, Reuter K. A practical guide to surface kinetic Monte Carlo simulations. *Front Chem.* 2019:*7*;202.

181. Stamatakis M, Vlachos, DG. A graph-theoretical kinetic Monte Carlo framework for on-lattice chemical kinetics. *J Chem Phys.* 2011:*134*;214115.

182. Stamatakis M, Vlachos DG. Unraveling the complexity of catalytic reactions via kinetic Monte Carlo simulation: Current status and frontiers. *ACS Catal.* 2012:*2*;2648-2663.

183. Prats H, Illas F, Sayós R. General concepts, assumptions, drawbacks, and misuses in kinetic Monte Carlo and microkinetic modeling simulations applied to computational heterogeneous catalysis. *Int J Quantum Chem.* 2018:*118*;e25518.

184. Heiber MC. KMC_Lattice v2.0: An object-oriented C++ library for custom kinetic Monte Carlo simulations. *J Open Source Softw.* 2019:*4*;1168.

185. Ritchie H, Roser M. United States: Cumulative: how much CO_2 has it produced to date?, Our World in Data, Available at: https://ourworldindata.org/co2/country/united-states#cumulative-how-much-co2-has-it-produced-to-date, Accessed 14 January 2021.

186. Annual Energy Outlook 2020, Independent Statistics &Analysis - U.S. Energy Information Administration, Available at: https://www.eia.gov/aeo, Accessed 14 January 2021.

187. EIA projects nearly 50% increase in world energy usage by 2050, led by growth in Asia, Independent Statistics &Analysis - U.S. Energy Information Administration, Available at: https://www.eia.gov/todayinenergy/detail.php?id=41433, Accessed 14 January 2021.

188. Lourenço MAO, Gomes JRB, Ferreira P. Gas-Organic and Gas-Inorganic Interfacial Effects in Gas/Adsorbent Interactions: The Case of CO_2/CH_4 Separation (Chapter 9), in (Eds.) Delville M-H, Tauber A. Hybrid Organic-Inorganic Interfaces: Towards Advanced Functional Materials (Vol. 1), Wiley-VCH: Weinheim, 2018.

189. Tao L, Choksi TS, Liu W, Pérez-Ramírez J. Synthesizing High-Volume Chemicals from CO_2 without Direct H_2 Input. *ChemSusChem.* 2020;*13*:6066-6089.

190. Frei MS, Capdevila-Cortada M, García-Muelas R, Mondelli C, López N, Stewart JA, Curulla Ferré D, Pérez-Ramírez J. Mechanism and microkinetics of methanol synthesis via CO_2 hydrogenation on Indium Oxide. *J Catal*. 2018;*361*:313−321.

191. Kondratenko EV, Mul G, Baltrusaitis J, Larrazabal GO. Pérez-Ramírez J. Status and perspectives of CO_2 conversion into fuels and chemicals by catalytic, photocatalytic and electrocatalytic processes. *Energy Environ Sci*. 2013;*6*:3112−3135.

192. Álvarez A, Borges M, Corral-Pérez JJ, Olcina JG, Hu L, Cornu D, Huang R, Stoian D, Urakawa A. CO_2 Activation over Catalytic Surfaces. *ChemPhysChem.* 2017;*18*:3135-3141.

193. Whang HS, Lim J, Choi MS, Lee J, Lee H. Heterogeneous catalysts for catalytic CO_2 conversion into value-added chemicals. *BMC Chem Eng.* 2019;*1*:9.

194. Dibenedetto A, Angelini A, Stufano P. Use of carbon dioxide as feedstock for chemicals and fuels: homogeneous and heterogeneous catalysis. *J Chem Technol Biotechnol.* 2014;*89*:334–353.

195. Cheng D, Negreiros FR, Aprà E, Fortunelli A. Computational Approaches to the Chemical Conversion of Carbon Dioxide. *ChemSusChem.* 2013;*6*:944-965.

196. Kong T, Jiang W, Xiong Y. Photocatalytic CO_2 conversion: What can we learn from conventional CO_x hydrogenation? *Chem Soc Rev*. 2020;*49*:6579-6591.

197. Gao F-Y, Bao R-C, Gao M-R, Yu S-H. Electrochemical CO_2-to-CO conversion: electrocatalysts, electrolytes, and electrolyzers. *J Mater Chem A.* 2020;*8*:15458-14578.

198. Nie X, Meng L, Wang H, Chen Y, Guo X, Song C. DFT insight into the effect of potassium on the adsorption, activation and dissociation of CO_2 over Fe-based catalysts. *Phys Chem Chem Phys* 2018;*20*:14694-14707.

199. Todorova TK, Schreiber MW, Fontecave M. Mechanistic Understanding of CO_2 Reduction Reaction (CO2RR) Toward Multicarbon Products by Heterogeneous Copper-Based Catalysts, *ACS Catal.* 2020;*10*:1754-1768.

200. Kolodziej A, Rodriguez P, Cuesta Ciscar A. Single-crystal Surfaces as Model Electrocatalysts for CO_2 Reduction (pp. 88-110). In (Eds.) Marken F, Fermin D. Electrochemical Reduction of Carbon Dioxide: Overcoming the Limitations of Photosynthesis, The Royal Society of Chemistry: Croydon, 2018.

201. Ko J, Kim B-K, Han JW. Density Functional Theory Study for Catalytic Activation and Dissociation of CO_2 on Bimetallic Alloy Surfaces. *J Phys Chem C.* 2016;*120*:3438-3447.

202. Pallassana V, Neurock M. Electronic factors governing ethylene hydrogenation and dehydrogenation activity of pseudomorphic Pd-ML/Re(0001), Pd-ML/Ru(0001), Pd(111), and Pd-ML/ Au(111) surfaces. *J Catal*. 2000;*191*:301-317.

203. Nørskov JK, Bligaard T, Logadottir A, Bahn S, Hansen LB, Bollinger M, Bengaard H, Hammer B, Sljivancanin Z, Mavrikakis M, Xu Y, Dahl S, Jacobsen CJH. Universality in heterogeneous catalysis. *J Catal.* 2002;*209*:275-278.

204. Liu ZP, Hu P. General rules for predicting where a catalytic reaction should occur on metal surfaces: A density functional theory study of C-H and C-O bond breaking/making on flat, stepped, and kinked metal surfaces. *J Am Chem Soc.* 2003;*125*:1958-1967.

205. Bader RF, *Atoms in Molecules: A Quantum Theory*, Oxford Science, Oxford, U.K., 1990.

206. Lozano-Reis P, Prats P, Gamallo P, Illas F, Sayós R. Multiscale Study of the Mechanism of Catalytic CO_2 Hydrogenation: Role of the Ni(111) Facets. *ACS Catal*. 2020;*10*:8077-8089.

207. Munnik P, de Jongh PE, de Jong KP. Recent Developments in the Synthesis of Supported Catalysts. *Chem Rev*. 2015;*115*:6687−6718.

208. Heiz U, Sanchez A, Abbet S, Schneider WD. Catalytic Oxidation of Carbon Monoxide on Monodispersed Platinum Clusters: Each Atom Counts. *J Am Chem Soc.* 1999;121:3214−3217.

209. Popok VN, Barke I, Campbell EEB, Meiwes-Broer KH. Cluster-Surface Interaction: From Soft landing to Implantation. *Surf Sci Rep.* 2011;66:347−377.

210. Yang XF, Wang A, Qiao B, Li J, Liu J, Zhang T. SingleAtom Catalysts: A New Frontier in Heterogeneous Catalysis. *Acc Chem Res.* 2013;*46*:1740-1748.

211. Yan C, Li H, Ye Y, Wu H, Cai F, Si R, Xiao J, Miao S, Xie S, Yang F, Li Y, Wang G, Bao X. Coordinatively unsaturated nickel–nitrogen sites towards selective and high-rate CO_2 electroreduction. *Energy Environ Sci.* 2018;*11*:1204-1210.

212. Jiang K, Siahrostami S, Zheng T, Hu Y, Hwang S, Stavitski E, Peng Y, Dynes J, Gangisetty M, Su D, Attenkoferf K, Wang H. Isolated Ni single atoms in graphene nanosheets for high-performance CO_2 reduction. *Energy Environ Sci.* 2018;*11*:893-903.

213. Akri M, El Kasmi A, Batiot-Dupeyrat C, Qiao B. Highly Active and Carbon-Resistant Nickel Single-Atom Catalysts for Methane Dry Reforming. *Catalysts* 2020;*10*:630.

214. Millet M-M, Algara-Siller G, Wrabetz S, Mazheika A, Girgsdies F, Teschner D, Seitz F, Tarasov A, Levchenko SV, Schlögl R, Frei E. Ni Single Atom Catalysts for CO_2 Activation. *J Am Chem Soc* 2019;*141*:2451–2461

215. Vogt C, Groeneveld E, Kamsma G, Nachtegaal M, Lu L, Kiely CJ, Berben PH, Meirer F, Weckhuysen BM. Unravelling structure sensitivity in CO_2 hydrogenation over nickel. *Nat Cata.l* 2018;*1*:127-134.

216. Zuo Z, Liu S, Wang Z, Liu C, Huang W, Huang J, Liu P. Dry Reforming of Methane on Single-Site Ni/MgO Catalysts: Importance of Site Confinement. *ACS Catal.* 2018;*8*:9821-9835.

217. Silaghi M-C, Comas-Vives A, Copéret C. CO_2 Activation on Ni/γ–Al2O3 Catalysts by First-Principles Calculations: From Ideal Surfaces to Supported Nanoparticles *ACS Catal.* 2016;*6*:4501-4505.

218. Kattel S, Yan B, Chen JG, Liu P. CO_2 hydrogenation on Pt, Pt/SiO_2 and Pt/TiO_2: Importance of synergy between Pt and oxide support. *J Catal.* 2016;*343*:115-126.

219. Levy RB, Boudart M. Platinum-like behavior of tungsten carbide in surface catalysis. *Science.* 1973;*181*:547-549.

220. Koverga AA, Flórez E, Dorkis L, Rodriguez JA. CO, CO_2, and H_2 interactions with (0001) and (001) tungsten carbide surfaces: importance of carbon and metal sites. *J Phys Chem C.* 2019;*123*:8871-8883.

221. Posada-Pérez S, Viñes F, Ramirez PJ, Vidal AB, Rodriguez JA, Illas F. The bending machine: CO_2 activation and hydrogenation on δ-MoC(001) and β-Mo_2C(001) surfaces. *Phys Chem Chem Phys.* 2014;*16*:14912-14921.

222. Kunkel C, Viñes F, Illas F. Transition metal carbides as novel materials for CO_2 capture, storage, and activation. *Energy Environ Sci.* 2016;*9*:141-144.

223. Posada-Pérez S, Viñes F, Rodriguez JA, Illas F. Fundamentals of methanol synthesis on metal carbide based catalysts: activation of CO_2 and H_2. *Top Catal.* 2015;*58*:159-173.

224. Liu Y, Tian D, Biswas AN, Xie Z, Hwang S, Lee JH, Meng H, Chen JG. Transition metal nitrides as promising catalyst supports for tuning CO/H_2 syngas production from electrochemical CO_2 reduction. *Angew Chem Int Ed.* 2020;*59*:11345-11348.

225. Rodriguez JA, Liu P, Gomes J, Nakamura K, Viñes F, Sousa C, Illas F. Interaction of oxygen with ZrC(001) and VC(001): Photoemission and first-principles studies. *Phys Rev B.* 2005;*72*:075427.

226. Dixit M, Peng X, Porosoff MD, Willauer HD, Mpourmpakis G. Elucidating the role of oxygen coverage in CO_2 reduction on Mo_2C. *Catal Sci Technol.* 2017;*7*:5521-5529.

227. Liu P, Rodriguez JA. Water-gas-shift reaction on molybdenum carbide surfaces: essential role of the oxycarbide. *J Phys Chem B.* 2006;*110*:19418–19425.

228. Viñes F, Rodriguez JA, Liu P, Illas F. Catalyst size matters: Tuning the molecular mechanism of the water–gas shift reaction on titanium carbide based compounds. *J Catal.* 2008;*260*:103–112.

229. Tominaga H, Nagai M. Density functional theory of water-gas shift reaction on molybdenum carbide. *J Phys Chem B.* 2005;*109*:20415-20423.

230. Kunkel C, Viñes F, Illas F. Surface activity of early transition-metal oxycarbides: CO_2 adsorption case study. *J Phys Chem C.* 2019;*123*:3664-3671.

231. López M, Viñes F, Nolan M, Illas F. Predicting the effect of dopants on CO_2 adsorption in transition metal carbides: Case study on TiC (001). *J Phys Chem C.* 2020;*124*:15969-15976.

232. López M, Broderick L, Carey JJ, Nolan M, Illas F. Tuning transition metal carbide activity by surface metal alloying: A case study on CO_2 capture and activation. *Phys Chem Chem Phys.* 2018;*20*:22179-22186.

233. Back S, Jung Y. TiC- and TiN-supported single-atom catalysts for dramatic improvements in CO_2 electrochemical reduction to CH_4. *ACS Energy Lett.* 2017;*2*:969-975.

234. Wang T, Liu X, Wang S, Huo C, Li YW, Wang J, Jiao H. Stability of β-Mo_2C facets from ab initio atomistic thermodynamics. *J Phys Chem C.* 2012;*116*: 6340−6348.

235. Prats H, Piñero JJ, Viñes F, Bromley ST, Sayós R, Illas F. Assessing the usefulness of transition metal carbides for hydrogenation reactions. *Chem Commun.* 2019;*55*:12797-12800.

236. Wannakao S, Artrith N, Limtrakul J, Kolpak AM. Engineering transition-metal-coated tungsten carbides for efficient and selective electrochemical reduction of CO_2 to methane. *ChemSusChem.* 2015;*8*:2745-2751.

237. Wannakao S, Artrith N, Limtrakul J, Kolpak AM. Catalytic activity and product selectivity trends for carbon dioxide electroreduction on transition metal-coated tungsten carbides. *J Phys Chem C.* 2017;*121*:20306-20314.

238 Rodriguez JA, Illas F. Activation of Noble Metals on Metal-Carbide Surfaces: Novel Catalysts for CO Oxidation, Desulfurization and Hydrogenation Reactions. *Phys Chem Chem Phys.* 2012;14:427-438.

239. Rodriguez JA, Viñes F, Illas F, Liu P, Takahashi Y, Nakamura K. Adsorption of gold on TiC(001): Au–C interactions and charge polarization. *J Chem Phys.* 2007;*127*:211102.

240. Florez E, Feria L, Viñes F, Rodriguez JA, Illas F. Effect of the support on the electronic structure of Au nanoparticles supported on transition metal carbides: Choice of the best substrate for Au activation. *J Phys Chem C.* 2009;*113*:19994-20001.

241. Gómez T, Florez E, Rodriguez JA, Illas F. Theoretical analysis of the adsorption of late transition-metal atoms on the (001) surface of early transition-metal carbides. *J Phys Chem C.* 2010;*114*:1622-1626.

242. Rodriguez JA, Liu P, Takahashi Y, Nakamura K, Viñes F, Illas F. Desulfurization of thiophene on Au/TiC(001): Au-C interactions and charge polarization. *J Am Chem Soc.* 2009;*131*:8595-8602.

243. Rodriguez JA, Liu P, Viñes F, Illas F, Takahashi Y, Nakamura K. Dissociation of SO_2 on Au/TiC(001): Effects of Au-C interactions and charge polarization. *Angew Chem Int Ed.* 2008;*47*:6685-6689.

244. Rodriguez JA, Ramírez PJ, Asara GG, Viñes F, Evans J, Liu P, Ricart JM, Illas F. Charge polarization at a Au-TiC interface and the generation of highly active and selective catalysts for the low-temperature water-gas shift reaction. *Angew Chem Int Ed.* 2014;*53*:11270-11274.

245. Vidal AB, Feria L, Evans J, Takahashi Y, Liu P, Nakamura K, Illas F, Rodriguez JA. CO_2 activation and methanol synthesis on novel Au/TiC and Cu/TiC catalysts. *J Phys Chem Lett.* 2012;*3*:2275-2280.

246. Posada-Pérez S, Ramírez PJ, Evans J, Viñes F, Liu P, Illas F, Rodriguez JA. Highly active Au/δ-MoC and Cu/δ-MoC catalysts for the conversion of CO_2: The Metal/C ratio as a key factor defining activity, selectivity, and stability. *J Am Chem Soc.* 2016;*138*:8269−8278.

247. Nilekar AU, Greelye J, Mavrikakis M. A simple rule of thumb for diffusion on transition-metal surfaces. *Angew Chem Int Ed.* 2006;*45*:7046-7049.

248 Naguib M, Kurtoglu M, Presser V, Lu J, Niu J, Heon M, Hultman L, Gogotsi Y, Barsoum MW. Two-Dimensional Nanocrystals Produced by Exfoliation of Ti_3AlC_2. *Adv Mater.* 2011;*4*:4248-4253.

249. Novoselov KS, Geim AK, Morozov SV, Jiang D, Zhang Y, Dubonos SV, Grigorieva IV, Firsov AA. Electric field effect in atomically thin carbon films. *Science*. 2004;*306*:666-669.

250. Deysher G, Shuck CE, Hantanasirisakul K, Frey NC, Foucher AC, Maleski K, Sarycheva A, Shenoy VB, Stach EA, Anasori B, Gogotsi Y. Synthesis of Mo_4VAlC_4 MAX phase and two-dimensional Mo_4VC_4 MXene with five atomic layers of transition metals. *ACS Nano.* 2020;*14*:204–217.

251. Ghidiu M, Lukatskaya MR, Zhao M-Q, Gogotsi Y, Barsoum MW. Conductive two-dimensional titanium carbide 'clay' with high volumetric capacitance. *Nature.* 2014;*516*:78-81.

252. Persson I, Halim J, Lind H, Hansen TW, Wagner JB, Näslund LÅ, Darakchieva V, Palisaitis J, Rosen J, Persson POÅ. 2D transition metal carbides (MXenes) for carbon capture. *Adv Mater.* 2019;*31*:1805472.

253. Kamysbayev V, Filatov AS, Hu H, Rui X, Lagunas F, Wang D, Klie RF, Talapin DV. Covalent surface modifications and superconductivity of two-dimensional metal carbide MXenes. *Science.* 2020;*369*:979-983.

254. Zhu J, Wang M, Lyu M, Jiao Y, Du A, Luo B, Gentle I, Wang L. Two-dimensional titanium carbonitride MXene for high-performance sodium ion batteries. *ACS Appl Nano Mater.* 2018;*12*:6854–6863.

255. Liu J, Peng W, Li Y, Zhang F, Fan X. 2D MXene-based materials for electrocatalysis. *Trans Tianjin Univ.* 2020;*26*:149-171.

256. Pang J, Mendes RG, Bachmatiuk A, Zhao L, Ta HQ, Gemming T, Liu H, Liu Z, Rummeli MH. Applications of 2D MXenes in energy conversion and storage systems. *Chem Soc Rev.* 2019;*48*:72-133.

257. Morales-García Á, Calle-Vallejo F, Illas F. MXenes: New horizons in catalysis. *ACS Catal.* 2020;*10*:13487-13503.

258. Kuang P, Low J, Cheng B, Yu J, Fan J. MXene-based photocatalysts. *J Mater Sci Technol.* 2020;*56*:18-44.

259. Peng J, Chen X, Ong WJ, Zhao X, Li N. Surface and heterointerface engineering of 2D MXenes and their nanocomposites: Insights into electro- and photocatalysis. *Chem.* 2019;*5*:18-50.

260. Hwu HH, Chen JG. Surface chemistry of transition metal carbides. *Chem Rev.* 2005;*105*:185-212.

261. Quesne MG, Roldan A, de Leeuw NH, Catlow CRA. Bulk and surface properties of metal carbides: implications for catalysis. *Phys Chem Chem Phy.s* 2018;*20*:6905-6916.

262. Dolz D, Morales-García Á, Viñes F, Illas F. Exfoliation energy as a descriptor of MXenes synthesizability and surface chemical activity. *Nanomaterials.* 2021;*11*:127.

263. Azofra LM, Li N, MacFarlane DR, Sun C. Promising prospects for 2D d^2–d^4 M_3C_2 transition metal carbides (MXenes) in N_2 capture and conversion into ammonia. *Energy Environ Sci.* 2016;*9*:2545-2549.

264. Gouveia JD, Morales-García Á, Viñes F, Gomes JRB, Illas F. Facile heterogeneously catalyzed nitrogen fixation by MXenes. *ACS Catal.* 2020;*10*: 5049–5056.

265. Morales-García A, Fernández-Fernández A, Viñes F, Illas F. CO_2 abatement using two-dimensional MXene carbides. *J Mater Chem A.* 2018;*6*:3381-3385.

266. Prats H, McAloone H, Viñes F, Illas F. Ultra-high selectivity biogas upgrading through porous MXenes. *J Mater Chem A* 2020;*8*:12296-12300.

267. Morales-García A, Mayans-Llorach M, Viñes F, Illas F. Thickness biased capture of CO_2 on carbide MXenes. *Phys Chem Chem Phys.* 2019;*21*:23136-23142.

268. Morales-Salvador R, Morales-García Á, Viñes F, Illas F. Two-dimensional nitrides as highly efficient potential candidates for CO_2 capture and activation. *Phys Chem Chem Phys* 2018;*20*:17117-17124.

269. Guo Z, Li Y, Sa B, Fang Y, Lin J, Huang Y, Tang C, Zhou J, Miao N, Sun Z. M_2C-type MXenes: Promising catalysts for CO_2 capture and reduction. *Appl Surf Sci.* 2020;*521*:14636.

270. Li N, Chen X, Ong WJ, MacFarlane DR, Zhao X, Cheetham AK, Sun C. Understanding of electrochemical mechanisms for CO_2 capture and conversion into hydrocarbon fuels in transition-metal carbides (MXenes). *ACS Nano.* 2017;*11*:10825-10833.

271. Kurlov A, Deeva EB, Abdala PM, Lebedev D, Tsoukalou A, Comas-Vives A, Fedorov A, Müller CR. Exploiting two-dimensional morphology of molybdenum oxycarbide to enable efficient catalytic dry reforming of methane. *Nat Commun.* 2020;*11*:4920.

272. Posada-Pérez S, Ramírez PJ, Gutiérrez RA, Stacchiola DJ, Viñes F, Liu P, Illas F, Rodriguez JA. The conversion of CO_2 to methanol on orthorhombic β-Mo_2C and Cu/β-Mo_2C catalysts: mechanism for admetal induced change in the selectivity and activity. *Catal Sci Technol.* 2016;*6*:6766-6777.

273 Jain A, Ong SP, Hautier G, Chen W, Richards WD, Dacek S, Cholia S, Gunter D, Skinner D, Ceder G, Persson KA. The Materials Project: A materials genome approach to accelerating materials innovation. *APL Materials* 2013; 1: 011002; see also https://materialsproject.org/

274 Draxl C, Scheffler M. The NOMAD laboratory: from data sharing to artificial intelligence. *J Phys Mater.* 2019;*2*:03600; https://nomad-coe.eu/

275. Winther KT, Hoffmann MJ, Boes JR, Mamun O, Bajdich M, Bligaard T. Catalysis-Hub.org, an open electronic structure database for surface reactions. *Sci Data.* 2019;*6*:75.

276. Ma S, Liu ZP. Machine learning for atomic simulations and activity prediction in heterogeneous catalysis: current status and future. *ACS Catal.* 2020;*10*:13213-13226.

277. Lamoureox PS, Winther KT, Garrido Torres JA, Streibel V, Zhao M, Bajdich M, Abild-Pedersen F, Bligaard T. Machine learning for computational heterogeneous catalysis. *ChemCatChem*. 2019;*11*:3581-3601.

278. https://www.go-fair.org/fair-principles/